Dalton Transactions

RSC Publishing

PAPER

View Article Online
View Journal

A novel $V^{IV}O$–pyrimidinone complex: synthesis, solution speciation and human serum protein binding†

Cite this: DOI: 10.1039/c3dt50553g

Gisela Gonçalves,[a] Isabel Tomaz,[a,e] Isabel Correia,[a] Luís F. Veiros,[a] M. Margarida C. A. Castro,[b] Fernando Avecilla,*[c] Lorena Palacio,[c] Miguel Maestro,[c] Tamás Kiss,[d] Tamás Jakusch,[d] M. Helena V. Garcia[e] and João Costa Pessoa*[a]

The pyrimidinones mhcpe, 2-methyl-3*H*-5-hydroxy-6-carboxy-4-pyrimidinone ethyl ester (mhcpe, **1**), 2,3-dimethyl-5-benzyloxy-6-carboxy-4-pyrimidinone ethyl ester (dbcpe, **2**) and *N*-methyl-2,3-dimethyl-5-hydroxy-6-carboxyamido-4-pyrimidinone (*N*-MeHOPY, **3**), are synthesized and their structures determined by single crystal X-ray diffraction. The acid–base properties of **1** are studied by potentiometric and spectrophotometric methods, the pK_a values being 1.14 and 6.35. DFT calculations were carried out to determine the most stable structure for each of the H_2L^+, HL and L^- forms (HL = mhcpe) and assign the groups involved in the protonation–deprotonation processes. The $mhcpe^-$ ligand forms stable complexes with $V^{IV}O^{2+}$ in the pH range 2 to 10, and potentiometry, EPR and UV-Vis techniques are used to identify and characterize the $V^{IV}O$–mhcpe species formed. The results are consistent with the formation of $V^{IV}O$, $(V^{IV}O)L$, $(V^{IV}O)L_2$, $(V^{IV}O)_2L_2H_{-2}$, $(V^{IV}O)L_2H_{-1}$, $(V^{IV}O)_2L_2H_{-3}$, $(V^{IV}O)LH_{-2}$ species and $V^{IV}O$-hydrolysis products. Calculations indicate that the global binding ability of mhcpe towards $V^{IV}O^{2+}$ is similar to that of maltol (Hmaltol = 3-hydroxy-2-methyl-4*H*-pyran-4-one) and lower than that of 1,2-dimethyl-3-hydroxy-4-pyridinone (Hdhp). The interaction of $V^{IV}O$-complexes with human plasma proteins (transferrin and albumin) is studied by circular dichroism (CD), EPR and ^{51}V NMR spectroscopy. $V^{IV}O$–mhcpe–protein ternary complexes are formed in both cases. The binding of $V^{IV}O^{2+}$ to transferrin (hTF) in the presence of mhcpe involves mainly $(V^{IV}O)_1$(hTF)$(mhcpe)_1$, $(V^{IV}O)_2$(hTF)$(mhcpe)_1$ and $(V^{IV}O)_2$(hTF)$(mhcpe)_2$ species, bound at the Fe^{III} binding sites, and the corresponding conditional formation constants are determined. Under the conditions expected to prevail in human blood serum, CD data indicate that the $V^{IV}O$–mhcpe complexes mainly bind to hTF; the formation of $V^{IV}O$–hTF–mhcpe complexes occurs in the presence of Fe^{III} as well, distinct EPR signals being clearly obtained for Fe^{III}–hTF and to $V^{IV}O$–hTF–mhcpe species. Thus this study indicates that transferrin plays the major role in the transport of $V^{IV}O$–mhcpe complexes under blood plasma conditions in the form of ternary V^{IV}–ligand–protein complexes.

Received 28th February 2013,
Accepted 15th April 2013

DOI: 10.1039/c3dt50553g

www.rsc.org/dalton

Introduction

The presence of vanadium in biological systems, its possible physiological roles and its therapeutic effects regarding its insulin-enhancing action and anticancer activity have driven a considerable amount of research. Particular interest has been devoted to the study of the potential benefits of vanadium compounds as insulin oral substitutes for the treatment of

[a]*Centro Química Estrutural, Instituto Superior Técnico, Universidade Técnica de Lisboa, Av. Rovisco Pais, 1049-001 Lisboa, Portugal. E-mail: joao.pessoa@ist.utl.pt; Fax: +351 218464455; Tel: +351 218419268*

[b]*Departamento de Ciências da Vida, Faculdade de Ciências e Tecnologia, Centro de Química de Coimbra e Centro de Neurociências e Biologia Celular, Universidade de Coimbra, 3000 Coimbra, Portugal*

[c]*Departamento de Química Fundamental, Universidaded de Coruña, Campus de A Zapateira s/n, 15071, A Coruña, Spain. E-mail: avecil@udc.es; Fax: +34 981167065; Tel: +34 981167065*

[d]*Department of Inorganic and Analytical Chemistry, University of Szeged, P.O. Box 440, Szeged H-6701, Hungary*

[e]*Centro de Ciências Moleculares e Materiais, Faculdade de Ciências da Universidade de Lisboa, Campo Grande, 1749-016 Lisboa, Portugal*

†Electronic supplementary information (ESI) available: ESI-1: Protonated–deprotonated forms of mhcpe calculated by DFT; ESI-2: experimental and calculated visible absorption spectra for the $V^{IV}O$–mhcpe system and discussion of the plausible binding modes; ESI-3: ternary systems $V^{IV}O$–amino acid–mhcpe; ESI-4: A 50 mm quartz cell for circular dichroism spectra measurements; ESI-5: circular dichroism spectra for the hTF–mhcpe system (UV range); ESI-6: CD spectra for the apo-hTF (and/or HSA)–$V^{IV}OSO_4$–mhcpe (or –maltol, or –dhp systems) in the UV range; ESI-7: CD spectra of solutions containing apo-hTF and additions of solutions containing $V^{V}O$–mhcpe complexes in the visible range; ESI-8: spectra of solutions containing apo-hTF, $V^{IV}OSO_4$, Fe^{III} and mhcpe; ESI-9: circular dichroism spectra of solutions containing HSA, $V^{IV}OSO_4$ and mhcpe – far UV range; ESI-10: synthesis of mhcpe (**1**), dbcpe (**2**), *N*-MeHOPY (**3**) and X-ray diffraction data. CCDC 926545 (**1**), 926546 (**2**) and 926547 (**3**). For ESI and crystallographic data in CIF or other electronic format see DOI: 10.1039/c3dt50553g

diabetes. Namely the role of the ligand has been a matter of debate: coordinated ligands should be able to improve the absorption in the gastrointestinal tract while also facilitating the transport and uptake of vanadium by the cells, reducing the dose necessary for producing an equivalent effect when compared to a vanadium salt/inorganic source.

Research has focused on the development of new and more efficient insulin-enhancing compounds as well as on understanding the mechanism of their action.[1–13] The mechanisms by which vanadium compounds mediate antidiabetic effects *in vivo* are not well understood. It is known that vanadate is a very potent inhibitor of phosphatases and other phosphorylases,[11,14–18] and the key events appear to involve interactions with protein tyrosine phosphatases and tyrosine kinases.[11,18–20] Several vanadium complexes have been found to have higher insulin enhancing activities than inorganic oxovanadium(v) or oxovanadium(iv) salts, but probably this improved efficacy probably relates to the increased bioavailability of the metal ion when involved in a complex rather than to increased potency at the phosphatase enzyme active sites.[19–23]

Among the several complexes exhibiting insulin enhancing properties, $V^{IV}O(maltolato)_2$ (BMOV) and $V^{IV}O(ethylmaltolato)_2$ (BEOV) have been extensively studied from the chemical and pharmacological points of view.[8,21–26] Complexes with 3-hydroxy-4-pyrones (3,4-HP) have also been extensively studied.[19,24–29]

Replacement of the O atom of the pyrone ring by a N or N–R group yields pyridinone derivatives, and both families of compounds maintain the (O^-, O^-) binding set, forming quite stable complexes with many metal ions.[28,30] Pyridinones have been proposed as oral therapeutic chelators for Fe^{III} and Al^{III} removal,[31,32] and the compound 1,2-dimethyl-3-hydroxy-4-pyridinone (Hdhp – Scheme 1), commercially known as Deferiprone®, is used in the treatment of β-thalassaemia.[31–33] The complexation of $V^{IV}O^{2+}$ and $V^{V}O_2^{+}$ with dhp was studied in aqueous solution[34–38] and exhibited quite interesting insulin like properties.[12,13,39,40]

Aiming at developing ligands with similar structural and binding ability characteristics of pyridinone and pyrone heterocycles, with improved aqueous solubility, we developed a distinct heterocyclic ligand system of the pyrimidinone type: 2-methyl-3*H*-5-hydroxy-6-carboxy-4-pyrimidinone ethyl ester, or mhcpe – Scheme 1 – containing two N atoms in the ring.[41]

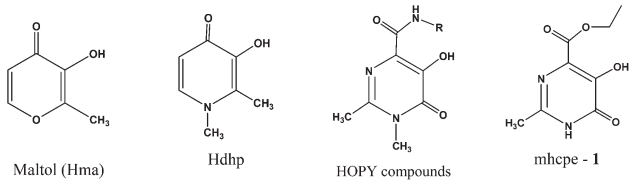

Scheme 1 Molecular formulas of maltol (Hma), Hdhp, 6-carboxamido-5,4-hydroxypyrimidinones (HOPY compounds) and mhcpe **1**. The totally protonated compounds correspond to HL, HL, H_2L^+ and H_2L^+, respectively. Unless a specific protonation state of **1** is needed, this compound will be designated by mhcpe. The same will be applied to the designations of maltol or dhp.

Pyrimidines, by virtue of substituting an additional carbon atom for a nitrogen atom in the heterocycle ring, reduce the capacity to tolerate the positive charge resulting from protonation and therefore may possess a more acidic protonation. However, depending on the nature and position of the substituting atoms of the ring, and the possibility of formation of intramolecular H-bonds, the actual protonation constants may be more or less basic than those of the corresponding pyridine compounds.

The system V^V–mhcpe was previously studied by pH-potentiometry and ^{51}V NMR by some of us, and its cytotoxic activity was screened with two different cell lines (HeLa tumor cells and 3T3-L1 fibroblasts).[42] The toxic effects were found to be incubation time and concentration dependent. According to the IC_{50} values and the results on reversibility to drug effects, the V^V–mhcpe system showed higher toxicity in the tumor cells than in non-tumor cells, which may indicate potential antitumor activity. In this work we report the synthesis and characterization of mhcpe, and the study of its interaction with $V^{IV}O^{2+}$ in aqueous anaerobic solution, using potentiometric and spectroscopic techniques.

It has been proposed that in higher organisms the delivery of vanadium into cells can be promoted by natural carriers such as plasma proteins, particularly by the high molecular mass (hmm) blood serum components: human serum transferrin (hTF) and human serum albumin (HSA).[22,23,40,43–50]

Transferrin (hTF) is a single-chain glycoprotein containing around 630 amino acids which are arranged in two similar lobes, and is important for iron transportation. It is present in human blood plasma in about 37 μM concentration. It has two binding sites per protein to accommodate Fe^{III}, one in each lobe, which is coordinated by two tyrosines, a histidine, an aspartate and a carbonate anion (the so-called synergistic anion) in a distorted octahedral geometry.[51] The binding mode of the metal ions at the two sites depends on the nature of the metal ion, the synergistic anion and the pH, but binding is generally slightly preferred at the C-terminal than at the N-terminal.[51] In normal serum, only about 30% of the total binding sites are occupied by iron.[7] This means that there are still sites available for other metal ions (corresponding to *ca.* 50 μM), without needing to replace the tightly bound Fe^{III}. In fact hTF can bind strongly to a range of other metal ions, as is the case of $V^{IV}O^{2+}$.[23,43,48–50]

Human serum albumin (HSA) is a globular protein consisting of a single polypeptide chain of 585 amino acids. It is the most abundant protein in plasma, accounting for ~60% of total plasma protein, with a concentration of *ca.* 0.63 mM, being the most important nonspecific transporter protein in the circulatory system.[52]

Since both albumin and transferrin play important roles in the distribution and transport of different compounds, they must be taken into account when evaluating the interactions and/or speciation of any metal-containing drugs once in human blood. Besides hTF and HSA other constituents should also be considered in any model which attempt to elucidate the fate of vanadium in human blood plasma. Strong evidence

has been provided to support that most of the vanadium in the serum is bound to hTF, even in the absence of HCO_3^-.[22,23,40,43,48–57] The results indicate that two vanadium ions are bound to the metal-ion-free apo-hTF, at the usual specific Fe^{III} binding sites. Under the physiological conditions, particularly in the hypothetical situation where the vanadium concentration is higher than *ca.* 50 μM, albumin may also participate in vanadium binding. If vanadium is introduced in blood in the form of a $V^{IV}O(carrier)_2$ complex (carrier = bidentate ligand), these carrier ligands and/or low molecular mass (lmm) bioligands may also participate in the transport of vanadium in blood.[23,40,43,45–50]

In this work we also report and discuss our findings by CD, EPR, and ^{51}V NMR spectroscopy regarding the interaction of V^V– and V^{IV}–mhcpe and vanadium–mhcpe complexes with human serum apo-transferrin (apo-hTF), as well as CD studies of interaction of V^{IV}-dhp and V^{IV}-maltol with apo-hTF and HSA in concentrations corresponding to those present in blood serum.

Results and discussion

Synthesis and characterization

The pyrimidinone mhcpe **1**, depicted in Scheme 1, was prepared as outlined in Scheme S-9-1† (see also the Experimental section), while dbcpe (**2**) was synthesized from one of the intermediates and *N*-MeHOPY (**3**) was obtained from **2**, as indicated in Scheme S-9-1.†[41] These compounds were characterized by ^1H and ^{13}C NMR, mass spectrometry and by single crystal X-ray diffraction, and their purity was confirmed by elemental analysis.

Crystals of **1** (mhcpe), **2** (dbcpe) and **3** (*N*-Me-HOPY), suitable for X-ray diffraction studies, were obtained. Ortep diagrams with the molecular structures are depicted in Fig. 1. In the crystals of mhcpe the N(1) atom is protonated and N(2) is not protonated. Atoms O(2)–H···O(3) are involved in intramolecular hydrogen bonds [O(2)–O(3) 2.628(3) Å, H(2O)–O(3) 1.91(4) Å and O(2)–H(2O)–O(3) 141(4)°] and every two molecules form a H-bonded dimer in the solid-state (see the ESI† section). Other intermolecular H-bonds are also observed: [N(1)–O(1) 2.837(4) Å, H(1A)–O(1) 1.98 Å, N(1)–H(1A)–O(1) 178.0° and O(2)–O(3) 3.113(4) Å, H(2O)–O(3) 2.42(4) Å, O(2)–H(2O)–O(3) 139(3)°]. In the crystal packing of mhcpe an offset-face-to-face (OFF) interaction is observed with a distance between the centres of both rings of 4.442 Å (Table 1).[58]

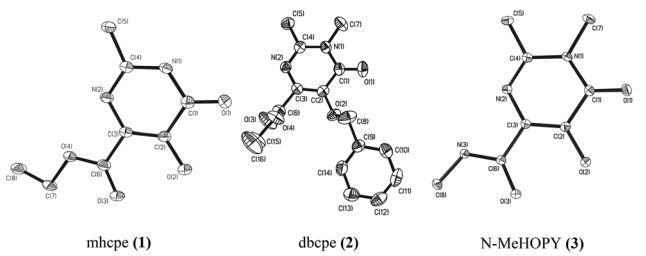

Fig. 1 Ortep diagrams (30% probability) of **1** (mhcpe), **2** (dbcpe) and **3** (*N*-MeHOPY), showing the atomic numbering scheme. For clarity hydrogen atoms are omitted.

Table 1 Selected bond lengths [Å] for **1** (mhcpe), **2** (dbcpe) and **3** (*N*-MeHOPY). Selected angles are given in the ESI† section

	1 – mhcpe	**2** – dbcpe	**3** – *N*-MeHOPY
Lengths (Å)			
O(1)–C(1)	1.222(4)	1.226(3)	1.2259(15)
O(2)–C(2)	1.330(3)	1.366(3)	1.3463(15)
O(3)–C(6)	1.196(4)	1.182(3)	1.2504(15)
O(4)–C(6)	1.317(4)	1.310(4)	
N(1)–C(4)	1.354(4)	1.374(3)	1.3798(16)
N(1)–C(1)	1.357(4)	1.393(4)	1.3965(16)
N(2)–C(4)	1.282(4)	1.302(3)	1.2962(16)
N(2)–C(3)	1.367(4)	1.359(4)	1.3740(15)
C(1)–C(2)	1.433(4)	1.442(4)	1.4549(17)
C(2)–C(3)	1.352(4)	1.357(4)	1.3634(17)
C(3)–C(6)	1.476(4)	1.502(4)	1.4878(16)
C(4)–C(5)	1.478(4)	1.488(4)	1.4913(18)

The solid state structure of dbcpe (**2**) has no hydrogen bond interactions. In the crystal of *N*-MeHOPY the hydrogen bond interactions differ from those of **1**. Aromatic–aromatic intermolecular interactions are present in the crystal packing of the crystals of mhcpe and of *N*-MeHOPY (see the ESI† section), and a comparative view of the π–π-stacking and hydrogen bonding interactions in the crystal packings of **1** (mhcpe) and of **3** (*N*-MeHOPY) is shown in Fig. S-10-3.†

Solution studies

Ethyl 5-hydroxy-2-methyl-6-oxo-1,6-dihydropyrimidine-4-carboxylate – mhcpe. The protonation equilibria were studied in the pH range of *ca.* 0.5 to 12 by UV absorption spectroscopy and in the pH range of *ca.* 1.8 to 12 by pH-potentiometry, at an ionic strength of 0.20 M KCl. Individual calibration curves of EMF *vs.* $[H^+]$ were established for pH values <~2, valid for the present medium and electrodes. For this purpose a set of HCl solutions were prepared with known H^+ concentrations, all with an ionic strength of 0.20 M. This calibration curve was used for all measurements below *ca.* pH 2.

Only two protonation steps were observed. Fig. 2 depicts several of the UV absorption spectra obtained. The protonation constants of the ligand were calculated with the PSEQUAD computer program[59] using both the experimental UV spectra and potentiometric titrations, and the results are included in Table 2. The calculated pK_a values from the UV spectra are: pK_{a1} = 1.14 and pK_{a2} = 6.34. The pK_{a2} calculated from the pH-metric titrations is 6.36.

^1H NMR titration studies carried out in the pH range 1–8 made with solutions containing mhcpe led to inconclusive results as to where the protonation–deprotonations took place as the protons on the mhcpe molecule did not afford relevant information in this regard. To better understand the protonation and deprotonation processes, a thorough conformational study was carried out for H_2L^+, HL and L^- by means of DFT calculations.[60] The stability of the several tautomers

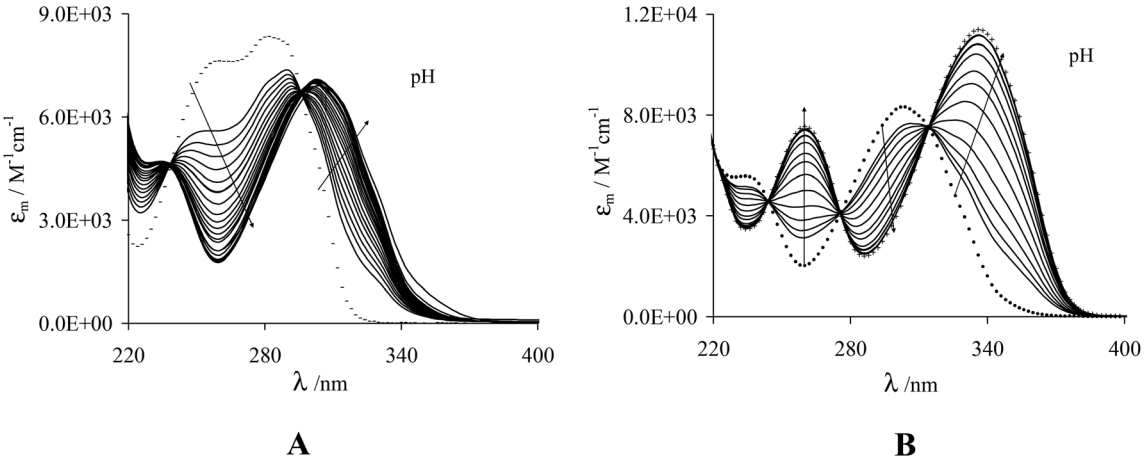

Fig. 2 UV spectra of *ca.* 10^{-4} M solutions of mhcpe, (A) pH 0.9 to 5.20; (B) pH 5.49 to 8.24; calculated UV spectra for (—) H_2L^+ (in A) and for (•••) HL and (+++) L^- species (in B) using the PSEQUAD program[59] are also included. The arrows indicate the spectral changes observed upon increasing the pH.

Table 2 Protonation and formation constants obtained from potentiometric and spectrophotometric data with the PSEQUAD computer program[59] for aqueous solutions containing mhcpe and $V^{IV}O(ClO_4)_2$ at 25 °C and I = 0.2 M KCl

H_nL	Log β	pK_a
HL	6.35 (±0.06)	6.35
H_2L	7.48 (±0.15)	1.14
$(VO)_pL_qH_r$	Log β ($V^{IV}O^{2+}$)[a]	
(VO)L	6.28 (±0.10)	
$(VO)L_2$	11.67 (±0.10)	
$(VO)L_2H_{-1}$	5.02 (±0.10)	~6.7
$(VO)_2L_2H_{-2}$	5.1 (±0.5)	
$(VO)_2L_2H_{-3}$	−0.08 (±0.2)	~5.2
$(VO)LH_{-2}$	−5.24 (±0.10)	

[a] The values given as (±x) for the vanadium complexes are not the standard deviations obtained directly by the PSEQUAD program; the values given account for the range in the log β values obtained in the several equilibrium models tested using the potentiometric and spectrophotometric data. These values are thus higher than the SDs given by the individual calculations of PSEQUAD.

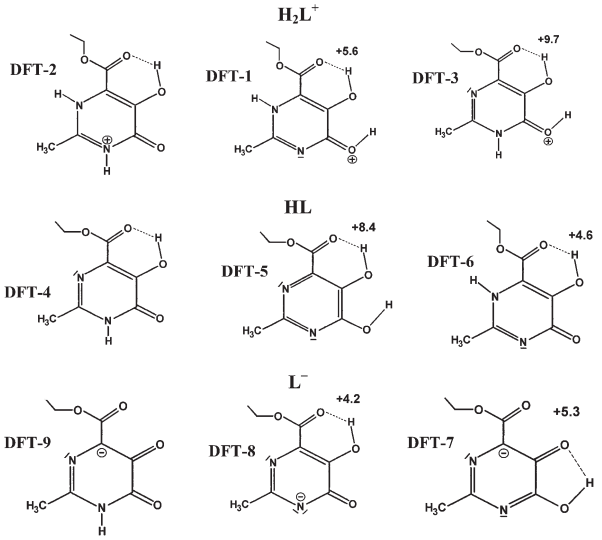

Scheme 2 The most stable structures calculated for H_2L^+ (top), HL (center), and L^- (bottom). Solvent (water) effects were considered in the energy calculations. The stability difference between tautomers (kcal mol^{-1}) is indicated for each stoichiometry, the structures depicted on the left side being the most stable ones for each protonation state.

considered may depend, to some extent, on solvation and ionic interactions occurring in solution. Since the solvent is water, solvation will rely on H-bonds established between the solute and solvent; as the comparison is made between isomers, part of the solvation effects are expected to cancel, and the energy differences calculated with implicit solvent corrections (PCM model, see the DFT computational details section) should give important clues to understand the predominant species in aqueous solution, in each case.

The structures of several tautomeric forms were calculated in a thorough search for each stoichiometry H_2L^+ (a total of 8 tautomers), HL (a total of 10 tautomers) and L^- (a total of 5 tautomers). The structures presented in Scheme 2 and discussed above correspond to the most stable tautomers, with energy differences less than 10 kcal mol^{-1} (see the section ESI-1†) with respect to the most stable tautomer of each stoichiometry. Additional metric and electronic parameters for the optimized structures are provided in the ESI† section, as well as the atomic coordinates for all optimized species. Partial charges and Wiberg indexes are also given in the section ESI-1.†

For 3-hydroxy-4-pyridinone derivatives there is some consensus in the literature that the protonation of the HL species takes place mainly on the N atom of the ring and the pK_{a1} values obtained, in the range 3.5–3.8, are several orders of magnitude higher than those for 3-hydroxy-4-pyrones.[28,35] This may be explained considering that in the H_2L^+ form of the compounds, the N atom is more efficient in delocalizing the positive charge in the ring than the O atom. Accordingly, for the H_2L^+ form of the pyrimidinone mhcpe the most stable form (**DFT-2** in Scheme 3) corresponds to the tautomeric form where both N-atoms are protonated. The tautomeric form

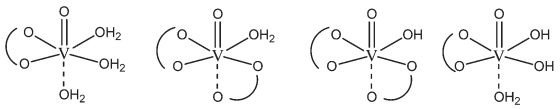

Scheme 3 Proposed binding modes for the monomeric complexes that form in the $V^{IV}O$–mhcpe system in aqueous solution (see the text and section ESI-2†).

where N(2) is protonated and N(1) is deprotonated (**DFT-1**) is less stable by 5.6 kcal mol^{-1}, and the form where atom N(2) is deprotonated and atom N(1) is protonated (**DFT-3**) is less favorable by +9.7 kcal mol^{-1}.

The pK_{a2} values obtained for pyridinones, in the range 9.7–9.9,[28,35] show that pyridinones are stronger bases than pyrones. This has been attributed to the delocalization of the partial negative charge to the O atom in position 4 of the ring.[28,35] For the HL species of mhcpe the most stable tautomer corresponds to the one characterized by X-ray diffraction. The tautomer with N(1) deprotonated and atom N(2) protonated is less stable by 4.6 kcal mol^{-1} (**DFT-6**), and the tautomer with both N atoms deprotonated is less favourable by 8.4 kcal mol^{-1} (**DFT-5**).

For the L^- species, the most stable tautomer corresponds to **DFT-9**, where the O-atoms that may coordinate to metal ions are not protonated. The other two tautomers present similar stabilities: in **DFT-8** (+4.2 kcal mol^{-1}) the negative charge is delocalized over the ring and atom O(1), and in **DFT-7** (+5.3 kcal mol^{-1}) the atom O(1) is protonated and the H-bond O(2)–H···O(3) is not present, but instead a relatively strong H-bond involving O(1)–H···O(2) is predicted (d_{OH-O} = 1.713 Å).

$V^{IV}O$–mhcpe complexes

Structure and binding constants. The mhcpe ligand binds $V^{IV}O^{2+}$ reasonably well at low pH. Fig. 3 includes visible spectra (Vis spectra) of solutions containing $V^{IV}O^{2+}$ and mhcpe with a ligand-to-metal molar ratio (L : M ratio) of 2.76. At low pH values, *e.g.* ~1.0, the UV-Vis spectra already differ from the spectrum of the free $V^{IV}O^{2+}$ ion (in fact: $[V^{IV}O(OH)_5]^{2+}$), namely in the 600–900 nm range, clearly indicating extensive complex formation at this pH. Band II ($d_{xy} \rightarrow d_{x^2-y^2}$) and charge-transfer bands progressively build up at ~480 nm, bathochromic effects being observed with an increase in pH, and band I ($d_{xy} \rightarrow d_{xz},d_{yz}$)[61] also increases its intensity and also shows a red shift up to pH = 6.68, as highlighted by the arrows in Fig. 3.

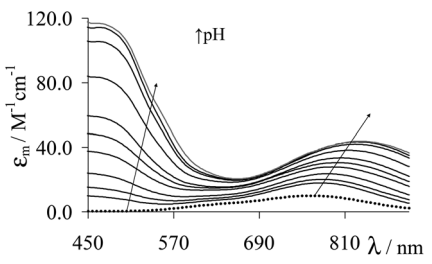

Fig. 3 Representative Vis absorption spectra recorded with aqueous solutions containing $V^{IV}O^{2+}$ and mhcpe at L : M = 2.76 and C_{VO} = 5 mM, upon increasing the pH from 0.98 to 6.68. The spectrum of $[V^{IV}O(H_2O)_5{}^{2+}]$ (•••) is also included for comparison.

Fig. S-2-1† includes representative Vis spectra for pH > 6.6. Globally the Vis spectra change significantly as the pH is increased particularly for pH > *ca.* 7, but do not change much in the pH range *ca.* 4.5–6.5. Moreover, while up to pH 7.2 the Vis spectra do not change much with changes in the L : M ratio [varying the C_{VO} from 2 to 6 mM keeping C_{mhcpe} approximately constant] indicating that no oligomeric species form, for pH > 7.5 similar types of experiments show changes indicating the formation of oligomeric species, and hydrolysis for pH > 8–9. The extension of the hydrolytic processes depends on the L : M ratio used.

The complex formation constants were calculated with the PSEQUAD computer program[59] from the potentiometric titration data at different C_{VO}, C_{mhcpe} and L : M ratios (see the Experimental section). The best model refined from experimental data includes stoichiometries (oxidation state and charges omitted for clarity): VO, (VO)L, $(VO)L_2$, $(VO)_2L_2H_{-2}$, $(VO)L_2H_{-1}$, $(VO)_2L_2H_{-3}$ and $(VO)LH_{-2}$. The log β of a few other stoichiometries could be obtained in some calculations, but either they were obtained with high standard deviations (SD) and/or they were not obtained with consistent values and/or they did not improve the fitting parameter, and were thus ruled out.

The PSEQUAD computer program and the Vis spectra obtained under different conditions (C_{VO}, C_{mhcpe}, L : M ratios and pH values) were also used to calculate the log β and/or the spectrum of each individual species formed. The calculated log β values calculated from spectral data agree well with those obtained from the pH-potentiometry (within ±0.1 log unit), and Vis spectra (included in the ESI† section) in agreement with the experimental data recorded could be calculated for almost all species included in the equilibrium model; this confirms that the speciation model proposed and the log β values calculated are correct and reliable. These data are included in Table 2 and a concentration distribution diagram is presented in Fig. 4.

It is clear from the speciation diagram that the mhcpe ligand forms quite stable complexes with $V^{IV}O^{2+}$ in a wide pH range, its hydrolytic products only forming in measurable concentration for pH > 7.5. At pH ~ 7 $V^{IV}O^{2+}$ is chelated in solution by mhcpe as $(V^{IV}O)L_2$, $[(V^{IV}O)L_2H_{-1}]^-$, and $[(V^{IV}O)_2L_2H_{-3}]^-$ complexes. The pK_a of the process $(V^{IV}O)L_2 \rightleftarrows (V^{IV}O)L_2H_{-1}{}^- + H^+$, corresponding to *ca.* 6.7, suggests the deprotonation of a coordinated water molecule from $(V^{IV}O)L_2$, and an OH^- is thus expected in the coordination sphere of $[(V^{IV}O)L_2H_{-1}]^-$. The Vis spectra calculated for each stoichiometry with PSEQUAD are consistent with experimental data and are obtained with good SDs and fitting parameters. Only for the $(VO)_2L_2H_{-2}$ stoichiometry the Vis spectra calculated show some parts with a negative extinction coefficient (*i.e.* negative values for ε_{22-2}, not shown) which is most likely due to the low concentration of this species under all experimental conditions used; thus it is not surprising that the Vis spectrum of $(VO)_2L_2H_{-2}$ cannot be/is not calculated adequately.

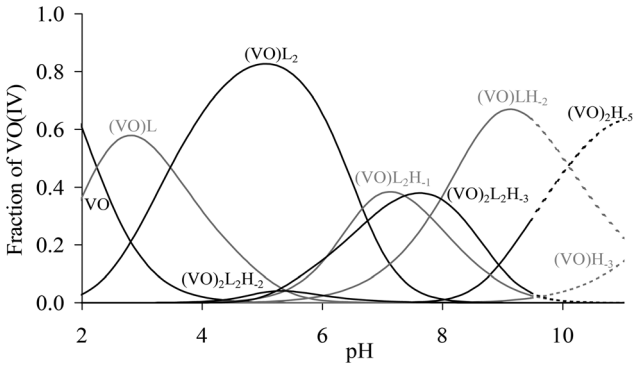

Fig. 4 Species distribution diagram for the complexes formed in the $V^{IV}O$–mhcpe system for solutions with C_{VO} = 5 mM and L : M = 2 (25 °C and I = 0.2 M KCl). Charges are omitted for simplicity. (VO) refers to the aquocomplex $[V^{IV}O(H_2O)_5]^{2+}$. Dotted lines above pH *ca.* 9 account for the lower accuracy of the formation constants for $V^{IV}O$-hydrolysis species $[(V^{IV}O)_2(OH)_5^-]_n \equiv (VO)_2H_{-5}$ and $[V^{IV}O(OH)_3^-] \equiv (VO)H_{-3}$.[61,62]

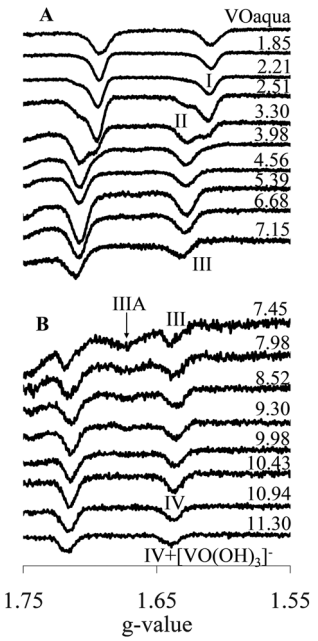

Fig. 5 High field region of the 1st derivative EPR spectra (77 K) of frozen aqueous solutions (with 5% DMSO) containing $V^{IV}O^{2+}$ and mhcpe at several pH values, A: $C_{VO} \approx 5$ mM and L : M = 3 and B: $C_{VO} \approx 4$ mM and L : M = 4. The spin Hamiltonian parameters obtained for species **I–IV** from simulation of the experimental spectra are presented in Table 3.

Plausible binding modes. EPR spectra were measured in "frozen" solution (77 K) to confirm the speciation model and to elucidate binding modes for each species. Some of the EPR spectra obtained for the $V^{IV}O$–mhcpe system, in the range corresponding to M_I = 5/2 and 7/2 (in the high field region of the spectrum), are depicted in Fig. 5. Table 3 summarises spin Hamiltonian parameters obtained in the $V^{IV}O$–mhcpe system from the simulation of the EPR spectra.[63]

Four main species, designated as **I–IV** and assigned to stoichiometries (VO)L, $(VO)L_2$, $(VO)L_2H_{-1}$ and $(VO)LH_{-2}$, can be identified as the pH is increased from 2 to 11 (Fig. 5, Table 3). The EPR spectral intensity decreases slightly in the pH range 4–6, and remarkably for pH > 7, in agreement with the formation of two dinuclear species: $(VO)_2L_2H_{-2}$ (present in very low concentration) and $(VO)_2L_2H_{-3}$, the latter probably being responsible for the broad weak feature detected at pH *ca.* 7.5 (at its maximum concentration) identified as **IIIA** in Fig. 5.[49,64] $V^{IV}O$-hydrolysis (accounted here by the formation of EPR-silent $[(V^{IV}O)_2(OH)_5^-]$ and EPR-active $[V^{IV}O(OH)_3^-]$) species[61,62] become important for pH > 9.5. At high pH (*ca.* 11), species **IV**, corresponding to $(V^{IV}O)L_2H_{-1}$, is probably superimposed by $[V^{IV}O(OH)_3^-]$ signals, which can be indicated by a slight decrease in the A_z value obtained in the simulation of the spectrum at pH = 11.30 (A_z^{est} for $[V^{IV}O(OH)_3^-] = 161.7 \times 10^{-4}$ cm^{-1}) and by a slight line broadening.

An additivity rule was developed for $V^{IV}O$-systems[11,65,66] to estimate the hyperfine coupling constant A_z^{est}, based on the contributions $A_{z,i}$ of each of the four equatorial donor groups $\{A_z^{est} = \Sigma A_{z,i}, i = 1 \text{ to } 4\}$, the estimated accuracy of A_z^{est} being ±3 × 10^{-4} cm^{-1}. No $A_{z,i}$ data have been presented in the literature[66] for ligands such as pyridones, pyridinones or pyrimidinones, but data are available for the contribution to A_z from the equatorial $O^{\delta-}$ (A_z^{O-}) for maltol[67] and other pyridinones.[28] For $(V^{IV}O)L_2$ complexes with bidentate ligands there is the possibility of the formation of at least two types of isomeric complexes: *cis*-$(V^{IV}O)L_2$ (three $O^{\delta-}$ donors bound equatorially and one axially) and *trans*-$(V^{IV}O)L_2$ (all $O^{\delta-}$ donors bound equatorially). These can be frequently distinguished by EPR and care must be taken when estimating correct values for A_z^{O-}.

In Scheme 3 we depict the most plausible binding modes for the present $V^{IV}O$–mhcpe system, and in the ESI† section we present a detailed discussion, based on the EPR data and additivity rule, of how we estimated A_z^{O-} values for the mhcpe ligand as well as a discussion on how these binding sets were established.

Table 3 Spin Hamiltonian parameters (g_z and A_z) obtained for the species formed in the $V^{IV}O$–mhcpe system in aqueous solution. The EPR parameters were obtained by simulation of the experimental EPR spectra recorded for frozen aqueous solutions (containing 5% DMSO) with the computer program of Rockenbauer and Korez.[63] $O^{\delta-}$ refers to the O-cathecolate type donors from the mhcpe ligand. Structures for the proposed binding modes are included in structures for the proposed binding, Scheme 3

Complex	EPR species	g_z	$A_z/\times 10^4$ cm^{-1}	Proposed binding set
$(VO)L \equiv [(V^{IV}O)L]^+$	**I**	1.937	178.6	$(O^{\delta-}, O^{\delta-}, 2 \times H_2O)_{equat}$
$(VO)L_2 \equiv [(V^{IV}O)L_2]$	**II**	1.942	171.3	$(3 \times O^{\delta-}, H_2O)_{equat}(O^{\delta-})_{axial}$
$(VO)L_2H_{-1} \equiv [(V^{IV}O)L_2(OH)]^-$	**III**	1.944	169.4	$(3 \times O^{\delta-}, HO^-)_{equat}(O^{\delta-})_{axial}$
$(VO)LH_{-2} \equiv [(V^{IV}O)L(OH)_2]^-$	**IV**	1.943	167.0	$(2 \times HO^-, 2 \times O^{\delta-})_{equat}$

Comparison of the binding ability of $V^{IV}O^{2+}$ to mhcpe, dhp and maltol

Considering the formation constants included in Table 2 for $V^{IV}O$–mhcpe complexes, and those for $V^{IV}O$–dhp[35] and $V^{IV}O$–maltol,[68] and taking into account the hydrolytic $V^{IV}O$-species and protonation constants of the ligands, the $-\log[V^{IV}O^{2+}]$ (= pVO) may be obtained, thus giving a measure of the binding ability of these ligands towards $V^{IV}O^{2+}$. The values calculated are plotted in Fig. 6. It may be seen that mhcpe and maltol have a quite similar binding ability towards $V^{IV}O^{2+}$ in the pH range 2–10, while that of dhp is significantly higher, particularly for $3 < pH < 6$.

Considering the role of the ligand as a carrier for the metal ion (improving its absorption and transport to the target tissues/cells) an adequate binding ability is critical: the ligand is expected to bind $V^{IV}O^{2+}$ (in this case) efficiently enough to prevent hydrolysis and other side-reactions while allowing its release when appropriate. In this context, maltol being a proven effective carrier ligand for $V^{IV}O^{2+}$, and mhcpe exhibiting a similar adequate binding ability, we also expect this ligand to release the metal ion in the presence of adequate competitive bioligands.

Ternary systems $V^{IV}O$–amino acid–mhcpe

Following administration (either oral or by intravenous injection), any pharmaceutical will eventually be transported and distributed within the living system by the blood. If a vanadium complex, *e.g.* of $V^{IV}O(carrier)_2$ type, as is the case of $V^{IV}O(mhcpe)_2$, is taken orally or injected, during its transport in the blood stream complex formation with the serum components must be considered, namely with (i) some of the lmm constituents (the most potent binders are probably the negatively charged O donor-containing ligands), such as lactate, phosphate, oxalate and citrate, designated here as ligands B, and with (ii) the hmm protein constituents, *e.g.* human serum albumin, immunoglobulin G and transferrin. In this work we mainly address the binding of vanadium–mhcpe to hTF.

As mentioned above, in iron bound hTF each lobe contains a distorted octahedral Fe^{III} binding site consisting of two Tyr, one His, one Asp residues, and one bidentate carbonate anion, the two binding sites being similar. To test the formation of ternary (and quaternary) $V^{IV}O$-complex species in solution, namely including the mhcpe ligand, some model systems (L-His, L-Tyr, L-Asp, Gly-L-His, Gly-L-Asp, L-Asp) were evaluated at pH *ca.* 7.2 by measuring their CD spectra in solution. Most of these results are included in the ESI-3† section.

The degree of complex formation in solutions only containing $V^{IV}O^{2+}$ and amino acids in the pH range 6–8 with L : M ratios up to 4 is usually low, $V^{IV}O$-hydrolytic products normally predominate and often $V^{IV}O(OH)_2$ precipitates.[61,62] Adding mhcpe to these solutions the degree of formation of $V^{IV}O$-hydrolytic species decreases significantly and ternary species typically form, probably $V^{IV}O$–mhcpe–amino acidato complexes. In fact, if mhcpe is added to solutions containing $V^{IV}O^{2+}$ and several amino acids, *e.g.* L-His and L-Asp, the CD signal in the visible range increases significantly and the pattern of the CD spectra differs from those observed for the $V^{IV}O$(amino acidato) or $V^{IV}O$(amino acidato)$_2$ complexes.[61,62,69–75] In Fig. 7 we present one such example: the intensity of the CD signal corresponding to spectrum c ($V^{IV}O$: mhcpe : L-His at 1 : 1 : 3 ratio) is much higher than in the absence of mhcpe, where $V^{IV}O^{2+}$ is extensively hydrolysed. Upon addition of L-Asp to the solution of spectrum c, the CD signal changes, yielding spectrum d, suggesting the formation of distinct optically active complexes. In section ESI-3† several similar experiments are also described. Globally these indicate that ternary $V^{IV}O$–mhcpe–LIG complexes significantly form when LIG is L-His or L-Asp, but not when LIG corresponds to L-Tyr, Gly-L-Asp, lactate or citrate.

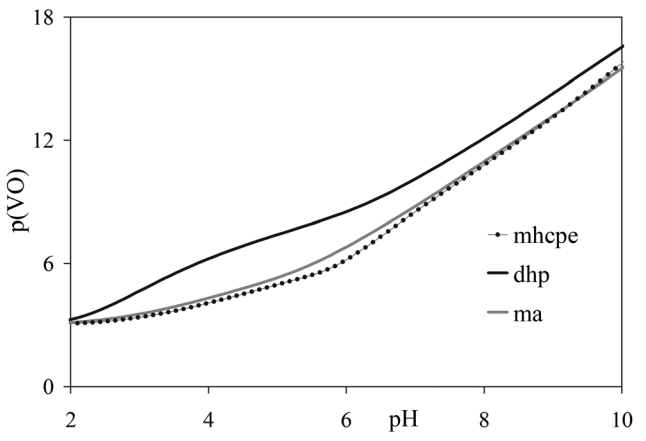

Fig. 6 Plot of $-\log[V^{IV}O^{2+}]$ (= pVO) for solutions containing $V^{IV}O$–mhcpe complexes, and those for $V^{IV}O$–dhp and $V^{IV}O$–maltol (see text). The plot was calculated taking C_{VO} = 1 mM and C_L = 2 mM, considering the formation constants obtained in this work and elsewhere.[35,68]

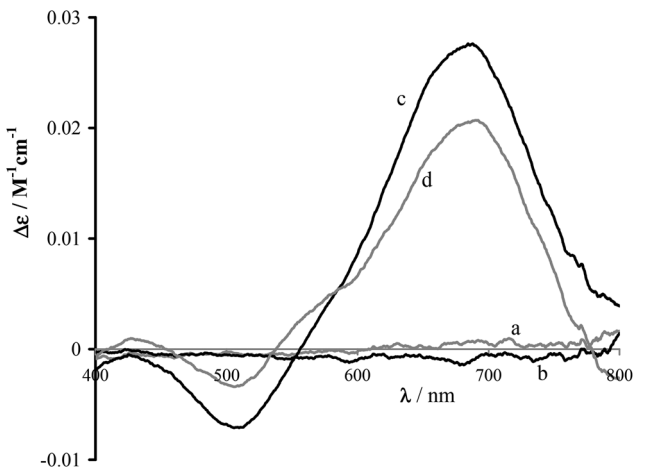

Fig. 7 CD spectra in the 400–800 nm range of solutions containing (a) L-His, (b) $V^{IV}O$: mhcpe : L-His = 1 : 1 : 3 at pH = 3.0, (c) $V^{IV}O$: mhcpe : L-His = 1 : 1 : 3 at pH = 7.2 and (d) $V^{IV}O$: mhcpe : L-His : L-Asp = 1 : 1 : 3 : 3 at pH = 7.2. The concentration of L-His or L-Asp is 6 mM (when present, $C_{VO} = C_{mhcpe}$ = 2 mM). The solvent is water and the optical path was 10 mm.

Interaction of vanadium–mhcpe complexes with apo-transferrin

CD spectroscopy is frequently used to monitor protein–drug interactions by following changes in the protein spectrum in the wavelength range 190–350 nm. In particular, the protein spectrum in the 200–250 nm range yields information on its secondary structure and on the changes it undergoes upon the binding of a compound, while the CD signal in the range 250–350 nm can be traced to the contribution from aromatic residues (Phe, Tyr, Trp) of the protein. Above 350 nm the protein is CD silent. However, in the case of the interaction of metal complexes, an induced CD signal (ICD) – resulting from chirality that is transmitted to metal-related electronic transitions – can be observed only if it binds in close proximity to chiral groups (this is what is observed in Fig. 9). The development of an ICD signal yields clear evidence of a strong interaction between the protein and the complex. The interaction of vanadium–mhcpe complexes with apo-human serum transferrin (hTF) was studied by monitoring the effect of both $V^{IV}O^{2+}$ (added as an inorganic salt) and complexes of $V^{IV}O$–mhcpe. Results on the interaction of mhcpe alone with the protein are included in the ESI† section (Fig. S-5-1 and S-5-2†).

CD spectra of solutions of apo-human serum transferrin (*ca.* 5 μM) at pH 7.4 practically do not change in the 200–250 nm range, where the protein has intrinsic electronic transitions, upon stepwise addition of $V^{IV}OSO_4$ up to a molar ratio of $V^{IV}O$: hTF of 1 : 1. However, upon further additions of $V^{IV}OSO_4$ up to a molar ratio of 10, the $|\Delta\varepsilon|$ increases (Fig. S-7-4†), although the global pattern of the CD spectra does not change. Part of these changes are probably due to the presence of V^{V}-species, formed by oxidation of $V^{IV}O$. In a similar experiment but upon stepwise additions of a solution containing $V^{IV}OSO_4$ and mhcpe in a 1 : 2 molar ratio at pH 7.4, the CD spectra also practically do not change up to a molar ratio of $V^{IV}O$: hTF of 2; further additions of $V^{IV}O(mhcpe)_2$ produced changes (Fig. S-7-5†) but much less pronounced than in the absence of mhcpe.

Upon the stepwise addition of mhcpe up to a mhcpe : hTF molar ratio of 10 : 1, $C_{hTF} \approx 100$ μM, in either Hepes-S or Hepes-CL buffer (CL buffer: similar to Hepes-S but also containing citrate and lactate, see the Experimental section), no significant changes are seen in the CD spectra in the 250–400 nm range (see Fig. S-5-1 and -2†). This means that mhcpe does not interact strongly with hTF under these experimental conditions. In contrast, if a 1 : 1 or 1 : 2 $V^{IV}O$: mhcpe solution is progressively added to apo-hTF, the CD spectra show important changes (see Fig. 8), particularly in the wavelength range 310–360 nm where the protein alone shows no CD signal.

The induced CD band at *ca.* 300–360 nm (centered at ~330 nm), clearly observed in Fig. 8, could be due to mhcpe absorption (see Fig. 2), and indicates that the mhcpe ligand is interacting closely with hTF; otherwise no CD band would be visible in this wavelength range. As this band is only observed when $V^{IV}O^{2+}$ and mhcpe are both present, this implies that

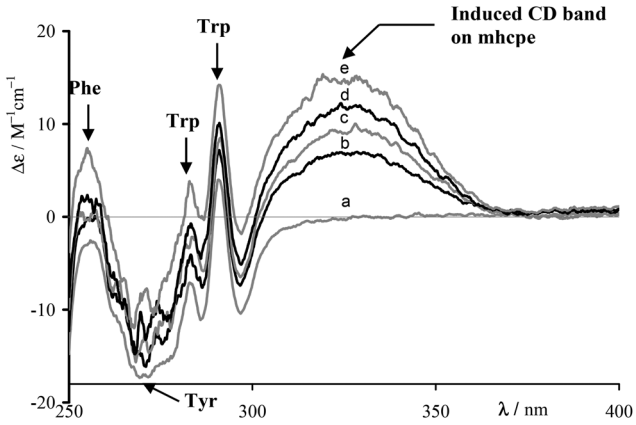

Fig. 8 CD spectra in the 250–400 nm range of solutions containing apo-hTF (C_{HTF} = 100 μM) and after stepwise additions of a solution containing $V^{IV}OSO_4$ and mhcpe in a 1 : 2 molar ratio in Hepes-CL buffer. (a) apo-hTF; (b) apo-hTF : $V^{IV}O$: mhcpe = 1 : 1 : 2; (c) apo-hTF : $V^{IV}O$: mhcpe = 1 : 2 : 4; (d) apo-hTF : VO : mhcpe = 1 : 3 : 6; (e) apo-hTF : VO : mhcpe = 1 : 6 : 12. The spectra were recorded with a 2 mm optical path quartz cell. For λ < 275 nm the optical density is too high; consequently the noise in the CD signal increases. Under similar conditions, the CD spectra of apo-hTF solutions (C_{hTF} = 100 μM) do not show significant changes up to a $V^{IV}O$: hTF molar ratio of 5, the spectra being equal to spectrum a.

mhcpe is also bound to $V^{IV}O$. Additional proof of this binding is given below. Similar measurements made in Hepes-S buffer (section ESI-6†) show very similar CD spectra, but the $\Delta\varepsilon$ values in the 320–360 nm range are *ca.* 25% higher, possibly because the citrate and lactate present in the Hepes-CL buffer partly sequester the $V^{IV}O^{2+}$, decreasing the amount bound to hTF. It is interesting to note that quite similar CD spectra, giving equivalent information, were obtained with solutions containing (i) $V^{IV}OSO_4$, maltol and apo-Tf and (ii) $V^{IV}OSO_4$, dhp and apo-hTF (section ESI-6†), thus also confirming the formation of ternary $V^{IV}O$–maltol–hTF and $V^{IV}O$–dhp–hTF complexes.[57]

Fig. 9 presents CD spectra (recorded with a 50 mm optical path quartz cell, see the section ESI-4†) in the 400–1000 nm range (designated here as the Vis range) of solutions containing apo-hTF and either (A) one equiv. or (B) two equiv. of $V^{IV}OSO_4$, and progressively adding mhcpe. All bands observed for λ > 500 nm correspond to d–d transitions of the V^{IV} center of the $V^{IV}O$ unit. In this wavelength range CD signals can only be observed if the $V^{IV}O$-species present are in close-interaction with chiral protein groups. Different CD signals must correspond to different types of V-species present and interacting with chiral protein groups.[61,62,69–73] Fig. 9 clearly shows that the $V^{IV}O$–protein CD spectra totally change upon adding mhcpe (spectra c–f), and therefore different $V^{IV}O$-species are formed. Namely, the pattern of the CD spectra corresponding to $(V^{IV}O)_1$(hTF) and $(V^{IV}O)_2$(hTF) complexes, due to one or two $V^{IV}O$-centres bound to apo-hTF in the iron binding sites, is no longer observed, thus implying that the mhcpe ligand binds to the $V^{IV}O$ centres which probably remain bound in the iron binding sites.

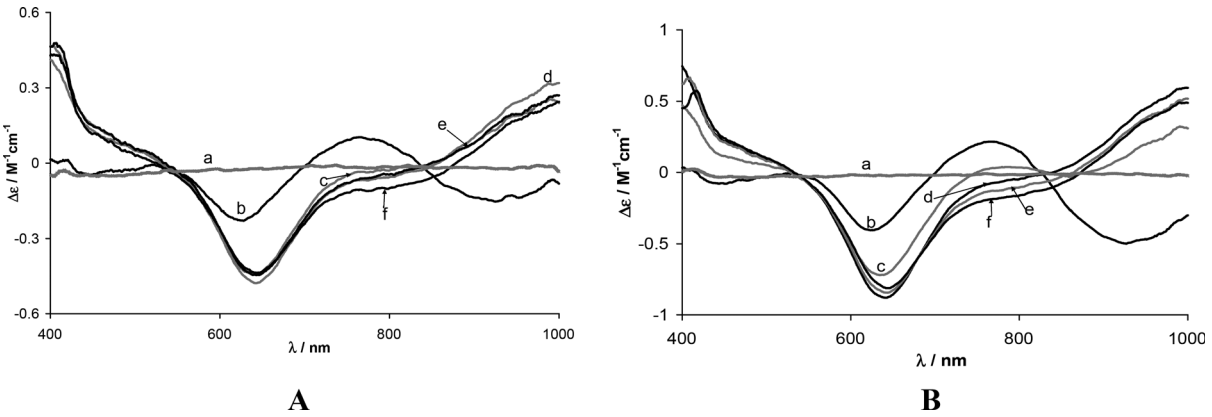

Fig. 9 CD spectra in the 400–1000 nm range of solutions in Hepes-S buffer containing (A) apo-hTF and $V^{IV}OSO_4$ ($C_{HTF} = C_{VO}$ = 750 μM) (a) apo-hTF; (b) apo-hTF : $V^{IV}O$: mhcpe = 1 : 1 : 0; (c) apo-hTF : $V^{IV}O$: mhcpe = 1 : 1 : 0.5; (d) apo-hTF : $V^{IV}O$: mhcpe = 1 : 1 : 1; (e) apo-hTF : $V^{IV}O$: mhcpe = 1 : 1 : 1.5; (f) apo-hTF : $V^{IV}O$: mhcpe = 1 : 1 : 2, and (B) apo-hTF and $V^{IV}OSO_4$ (C_{HTF} = 750 μM, C_{VO} = 2 × 750 μM), and progressively adding mhcpe (a) apo-hTF; (b) apo-hTF : $V^{IV}O$: mhcpe = 1 : 2 : 0; (c) apo-hTF : $V^{IV}O$: mhcpe = 1 : 2 : 0.5; (d) apo-hTF : $V^{IV}O$: mhcpe = 1 : 2 : 1; (e) apo-hTF : $V^{IV}O$: mhcpe = 1 : 2 : 1.5; (f) apo-hTF : $V^{IV}O$: mhcpe = 1 : 2 : 2. The spectra were recorded with a 50 mm optical path quartz cell (see the section ESI-4†).

The addition of up to 1.0 equiv. of mhcpe (relative to the $V^{IV}O$ present) causes a total change in the pattern of the ICD bands, namely the d–d bands Ib and Ia change signal, and band II becomes more negative,[61] but further additions of mhcpe do not change much the ICD bands measured. Quite similar CD spectra and trends were found when adding solutions containing either $V^{IV}OSO_4$ and mhcpe in 1 : 1 or 1 : 2 molar ratios to solutions containing apo-hTF at pH 7.4 (see the section ESI-7†). All observations suggest the formation of complexes with stoichiometries $(V^{IV}O)_1$(hTF)$(mhcpe)_1$, $(V^{IV}O)_2$(hTF)$(mhcpe)_1$ and $(V^{IV}O)_2$(hTF)$(mhcpe)_2$.

Fig. 10 depicts several EPR spectra of frozen solutions containing apo-hTF and $V^{IV}OSO_4$, and of solutions containing apo-hTF, $V^{IV}OSO_4$ and mhcpe. The EPR spectra differ when the mhcpe ligand is present, as was observed with the CD spectra (above), clearly indicating that a modification of the $V^{IV}O$-binding set changes when mhcpe is added to solutions containing apo-hTF and $V^{IV}OSO_4$. The number of distinct species detected and spin-Hamiltonian parameters do change, but as most donor groups give rather similar contributions to the g_z and A_z values, the modifications observed on the spectral lines are not drastic. Moreover, in the case where mhcpe is present we can observe the presence of the two new environments that we have labelled C and D, characterized by distinct A_z values (Table 5). The environment corresponding to C appears to be preferred over D. This behaviour was observed in both buffers, Hepes-S and Hepes-CL (the *g* and *A* values in both are equal), but the formation of D is slightly enhanced when the Hepes-CL buffer is used.

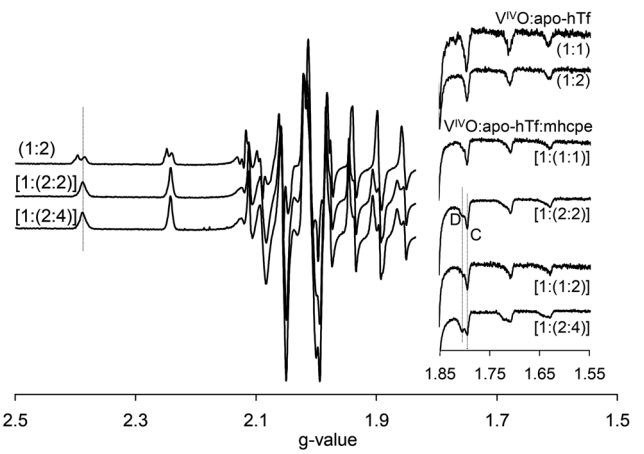

Fig. 10 First derivative EPR spectra of frozen solutions of apo-hTF (C_{hTF} = 750 μM) and $V^{IV}OSO_4$ ($C_{VO} = 2 \times C_{hTF}$), labeled 1 : 2, and of solutions containing apo-hTF ($C_{hTF} \approx 0.75$ mM), $V^{IV}OSO_4$ ($C_{VO} = 2 \times C_{hTF}$) and mhcpe ($C_{mhcpe} = C_{VO}$ or $C_{mhcpe} = 2 \times C_{VO}$), labeled 1 : (2 : 2) and 1 : (2 : 4). All solutions contain the Hepes-CL buffer at pH ~ 7.4. In the high-field region amplifications of the spectra are included, all with solutions containing apo-hTF ($C_{hTF} \approx 0.75$ mM) and with concentrations of $V^{IV}OSO_4$ and mhcpe according to the molar ratios indicated.

Calculation of conditional stability constants. The stability constants of the $(V^{IV}O)$–hTF and $(V^{IV}O)_2$–hTF species were determined[40] from the CD spectra and the isotropic/anisotropic EPR signal ratios with the computer program PSEQUAD[59] as: log K_1 = log β_1 = 13.4 and log K_2 = 11.9 (log β_2 = 25.3), respectively; these are conditional stability constants only valid at pH 7.4. Sanna *et al.*[76] obtained similar log β_1 and log β_2 values.

The stability constants of the ternary species $(V^{IV}O)_p$(hTF)$_1$$(mhcpe)_r$ were determined from the experimental CD spectra with different $V^{IV}O$–hTF–mhcpe molar ratios, also using the computer program PSEQUAD. The protonation constants of the ligands, the stability constants of the $V^{IV}O$–mhcpe complexes, and the hydrolytic constants of $V^{IV}O$ were all taken into account as fixed parameters in the calculations. The conditional stability constants for the binary species $(V^{IV}O)$–hTF and $(V^{IV}O)_2$–hTF were also considered with the known values. The stability constants calculated are presented in Table 4, and a speciation profile is depicted in Fig. 11 for an hTf concentration close to that of the human plasma. The

Table 4 Conditional formation constants[a] determined for the ternary $[(V^{IV}O)_p(hTF)_q(mhcpe)_r]$ system (p, r = 0–2; q = 1) using CD data and the computer program PSEQUAD[59] (in Hepes-S buffer at pH 7.4 and t = 25 °C)

$(VO)_p(hTF)_q(mhcpe)_r$	Composition (p,q,r)	Log β_{pqr}
(VO)(hTF)	(1,1,0)	13.37
$(VO)_2$(hTF)	(2,1,0)	25.21
(VO)(hTF)(mhcpe)	(1,1,1)	18.2(2)[b]
$(VO)_2$(hTF)(mhcpe)	(2,1,1)	31.0 (1)[b]
$(VO)_2$(hTF)$(mhcpe)_2$	(2,1,2)	35.5 (1)[b]

[a] For the definition of 'conditional formation constants' used, see the Experimental section. [b] The values given between parentheses are the standard deviations obtained directly by the PSEQUAD program multiplied by three.

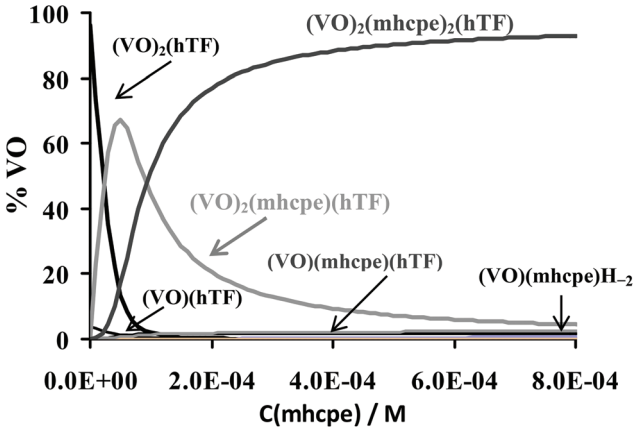

Fig. 11 Species distribution diagram for the complexes formed at pH 7.4 in the $V^{IV}O$–apo-hTF–mhcpe system for blood plasma conditions ($C_{apo-hTF}$ = 40 μM and C_{VO} = 80 μM), based on the stability constants presented in Table 5.

corresponding CD spectra were also calculated and are shown in Fig. S-7-3.† As expected, the profiles observed for the calculated CD spectra for the $V^{IV}O$–hTF or $V^{IV}O$–hTF–mhcpe species differ significantly, indicating a very distinct environment of $V^{IV}O$ in the presence and in the absence of the mhcpe ligand.

Several questions remain open, *e.g.* whether ternary or quaternary $V^{IV}O$-complexes form, which hTF donor groups/residues bind to the metal centre and if hTF can assume (or not) the closed conformation recognizable by the transferrin receptor in the presence of mhcpe (probably yes).[57]

Interaction of vanadium–mhcpe complexes with transferrin in the presence of iron

As mentioned above, in normal serum, only about 30% of the total Fe^{III} binding sites are occupied by this metal ion. As the hTF concentration in blood serum is *ca.* 37 μM this means that there are sites available for binding other metal ions, corresponding to *ca.* 50 μM, with no need to replace the tightly bound Fe^{III}. Therefore, hTF can also bind strongly to a range of other metal ions, as is indeed the case of $V^{IV}O^{2+}$.

In solutions containing $V^{IV}O^{2+}$ and hTF under conditions where there are enough free available sites for the binding of all $V^{IV}O^{2+}$ present, we observed that this metal ion is more easily oxidized to V^{V} than in the absence of Fe^{III}. This is an interesting observation considering that V^{IV} binds to hTF much more strongly to hTF than V^{V}.[40,47] A similar effect was observed in solutions also containing mhcpe, maltol or dhp. Fig. SI-8-1† includes CD spectra of solutions containing apo-hTF and after stepwise additions of a solution containing $V^{IV}O^{2+}$ and mhcpe with a 1 : 2 molar ratio. These spectra are similar to those presented in Fig. 9. Upon adding a solution containing an amount of Fe^{III} equivalent to 30% of the hTF Fe^{III}-binding sites, the ICD bands in the 500–1000 nm range, assigned to $V^{IV}O$ d–d transitions, decrease continuously with time due to the relatively fast oxidation of $V^{IV}O$- to V^{V}-species (Fig. SI-8-1†). This relatively fast oxidation occurs despite the hTF present in solution contains enough binding sites to bind all $V^{IV}O$ and Fe^{III} added.

Table 5 Spin Hamiltonian parameters (g_z and A_z) obtained for the species formed in the $V^{IV}O$–apo-hTF–mhcpe–Fe system in aqueous solutions containing the Hepes-S buffer at pH 7.4. The EPR parameters were obtained by simulation of the experimental EPR spectra recorded for frozen aqueous solutions with the computer program of Rockenbauer and Korez[59]

EPR species	g_z	A_z ($\times 10^4$ cm^{-1})
A	1.938	167.7
A[a]	1.938	168.0
A[b]	1.937	168.3
B	1.940	170.7
B[a]	1.938	170.0
B_1[b]	1.941	170.3
B_1[c]	1.941	170.5
B_2[b]	1.937	172.4
B_2[c]	1.935	171.8
C[d]	1.941	170.4
D[d]	1.946	166.5
E (contains Fe^{III})	1.941	168.2

[a] From Mustafi *et al.*[77] [b] From Chasteen *et al.*[78] [c] From Jakusch *et al.*[40] [d] The spin Hamiltonian parameters (g_z and A_z) obtained for these species are identical in measurements in Hepes-S and Hepes-CL buffers.

In Fig. 12 spectrum 1 corresponds to the EPR spectrum of a frozen solution containing apo-hTF (C_{hTF} = 0.75 mM), $V^{IV}OSO_4$ (C_{VO} = 1.50 mM) and Fe^{III} (C_{Fe} = 0.45 mM) at pH 7.4; the presence of both the $V^{IV}O$–hTF and Fe^{III}–hTF EPR signals is clearly seen. An EPR spectrum very similar to this one was recorded with a solution containing apo-hTF and $V^{IV}OSO_4$ (1 : 2 molar ratio), and upon addition of Fe^{III} to this solution. The Fe^{III} added removed an equivalent amount of $V^{IV}O^{2+}$ from the hTF Fe-binding sites and the intensity of the $V^{IV}O$-EPR spectrum decreased accordingly. The excess $V^{IV}O$ removed by the addition of Fe^{III} or that present in the bulk solution of spectrum 1 of Fig. 12 is not detected as it is in the form of EPR silent species and/or was oxidized to vanadate species.[61,62]

Upon addition of mhcpe the $V^{IV}O$-EPR spectrum changes due to the formation of $V^{IV}O$–hTF–mhcpe complexes. As mentioned above, in the presence of Fe^{III} the ICD spectra in the visible range decrease rather fast and the intensity of the $V^{IV}O$-EPR progressively decreases accordingly. The Fe^{III}-EPR spectra show some changes probably due to the formation of Fe^{III}–mhcpe complexes.

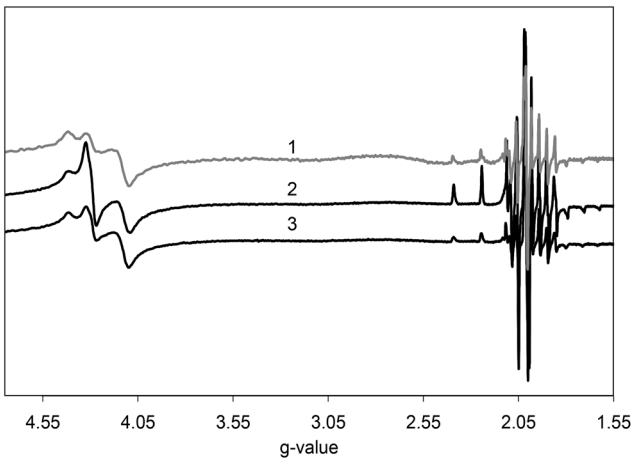

Fig. 12 First derivative EPR spectra of frozen solutions containing (1) apo-hTF (C_{hTF} = 0.75 mM), $V^{IV}OSO_4$ (C_{VO} ~ 1.50 mM) and Fe^{III} (C_{Fe} = 0.45 mM) in Hepes-S buffer, the hTF : $V^{IV}O$: Fe^{III} molar ratio thus being 1 : 2 : 0.6; (2) a solution of CD spectrum 5 of Fig. S-8-1;† (3) a solution of CD spectrum 11 of Fig. S-8-1,† *i.e.* the same solution after 1 h. See also spectra 1–3 of Fig. 13.

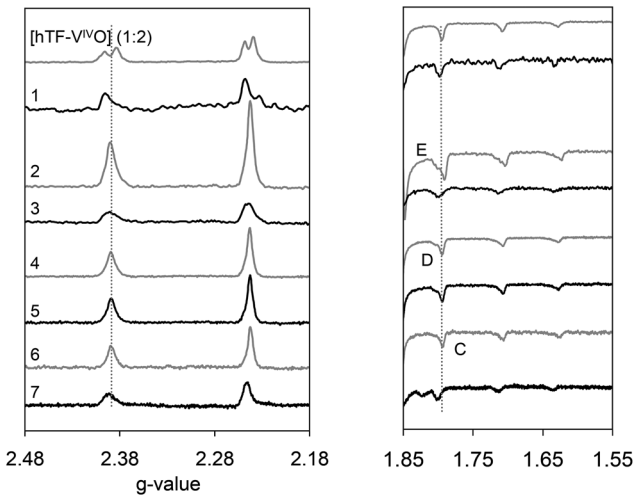

Fig. 13 Amplification of the low and high field ranges of the first derivative EPR spectra of frozen solutions containing the reagents indicated for each spectrum, $C_{hTF} \approx 0.75$ mM, in Hepes-S buffer of pH = 7.4 (see also Fig. S-8-2 and -3†). (1) [hTF : $V^{IV}O$: Fe] (1 : 2 : 0.6); (2) [hTF : $V^{IV}O$: mhcpe : Fe] (1 : 1.4 : 2.8 : 0.6); (3) [hTF : $V^{IV}O$: mhcpe : Fe] (1 : 1.4 : 2.8 : 0.6) t = 60 min; (4) [hTF : $V^{IV}O$: mhcpe] (1 : 1.4 : 2.8); (5) [hTF : $V^{IV}O$: mhcpe] (1 : 1 : 2); (6) [hTF : $V^{IV}O$: mhcpe] (1 : 0.6 : 1.2); (7) [$V^{IV}O$: mhcpe] (1 : 2) C_{VO} = 1 mM. All spectra correspond to solutions frozen shortly after their preparation (except spectrum 3). The corresponding 1st derivative EPR full spectra are depicted in Fig. S-8-2.† Spectra 1–3 are amplifications of the $V^{IV}O$-EPR spectra of Fig. 12 (with the same numbering). The spin Hamiltonian parameters obtained by simulation of these EPR spectra are summarized in Table 5.

The ^{51}V NMR spectrum of the solution of spectrum 3 of Fig. 12 was also measured and two resonances were observed: the signal corresponding to V^V–hTF species (at $\delta = -532$ ppm) and a low intensity signal corresponding to V^V–mhcpe complexes[42] (at $\delta \approx -538$ ppm). This means that upon addition of Fe^{III} to the solution containing apo-hTF and $V^{IV}O^{2+}$, in a 1 : 2 molar ratio, the $V^{IV}O^{2+}$ is oxidized to some extent to V^V-species which in turn bind to hTF. In the ESI† section additional information regarding EPR and ^{51}V NMR spectra measured is included.

Upon addition of Fe^{III} to solutions containing apo-hTF and $V^{IV}OSO_4$ (1 : 2) – spectrum 1 of Fig. 13, the $V^{IV}O$-EPR spectrum changes significantly: (i) the global intensity decreases, (ii) the relative intensity of resonances assigned to the $V^{IV}O$ binding to the C-terminal site (the B component in the $V^{IV}O$-EPR spectrum, see Fig. 15 and 16, which binds Fe^{III} more strongly) decreases drastically. Comparing the $V^{IV}O$-EPR spectra 2 and 3 of Fig. 13 (with [hTF : $V^{IV}O$: mhcpe : Fe] = 1 : 1.4 : 2.8 : 0.6 just after the Fe^{III} addition, and the same sample recorded 60 min later), it may be noticed that: (i) the intensity decreases significantly, this being compatible with oxidation of part of the $V^{IV}O$ present; and (ii) the A_z values slightly decrease. From observation of spectra 2 and 4–6 of Fig. 13 it can also be concluded that the spin-Hamiltonian parameters of the species present are slightly different, suggesting the presence of new species, designated by C and D, distinct from those detected in solutions of $V^{IV}O^{2+}$ and mhcpe at pH ≈ 7.4 (*e.g.* spectrum 7). No ^{51}V NMR signal corresponding to any hTF–V^V–mhcpe species was detected in this or in other experiments.

In Table 5 the spin Hamiltonian parameters obtained for the species formed in the $V^{IV}O$–apo-hTF–mhcpe–Fe system are summarized. The EPR signal corresponding to the $V^{IV}O$-species E differs significantly from those labelled as C or D, but corresponds to parameters very similar to those of A (or B), assigned to ($V^{IV}O$)–hTF species. However, it is not likely that they indeed correspond to $(V^{IV}O)_n$–hTF complexes as the CD spectrum measured differs from those of $(V^{IV}O)_n$–hTF complexes. We believe that this corresponds to a distinct complex, not previously detected; a possible assignment is the formation of a $V^{IV}O$–hTF bound species involving vanadate as a synergistic anion.

The reason why in the presence of Fe^{III} the spectroscopic CD and EPR signals of $V^{IV}O$ present disappear relatively fast (much faster than in its absence) is not clear. A plausible explanation is that in the presence of Fe^{III} some of the $V^{IV}O$ is removed from the stronger hTF binding sites, which increases the relative amount of $V^{IV}O$ not bound to the protein. As the pH of the solution is 7.4, this non-hTF-bound $V^{IV}O$ may be easily oxidized even if the amount of O_2 present is very low. If the amount of O_2 increases, *e.g.* by removing the stoppers of the cell, the oxidation proceeds much faster. Addition of glutathione to the solution does not promote the reduction of the V^V-species formed back to V^{IV} (see the ESI-8† section). This relatively fast oxidation in the presence of O_2 occurs even if there is enough hTF to bind all $V^{IV}O$ and all Fe^{III} present.

The implications of these observations for *in vivo* conditions cannot be anticipated easily. There are no reports stating that the oxidation of $V^{IV}O$ may proceed in blood. In contrast, it is usually assumed that $V^{IV}O$-species are stabilized and protected from oxidation by the presence of several biological reducing agents.[61,79] A possible explanation is that vanadate may act as a synergistic anion for Fe^{III} (and possibly also for $V^{IV}O$) binding to hTF, this being a driving force for the

partial oxidation of $V^{IV}O$. Further studies are being carried out to understand the processes taking place in these systems.

Interaction of vanadium–mhcpe complexes with human serum albumin

Fig. 14 depicts CD spectra of solutions containing HSA (grey spectrum, which may be considered as the baseline), and of solutions containing HSA, $V^{IV}OSO_4$ and mhcpe in the 400–1000 nm range. The CD spectra of solutions containing HSA and $V^{IV}OSO_4$ differ from those of solutions containing HSA, $V^{IV}OSO_4$ and mhcpe. Namely, the λ_{max} of the two main bands observed in the 400–1000 nm range differ, and the $|\Delta\varepsilon|$ values are much higher, by a factor of *ca.* 7, when mhcpe is present in solution. The rather high $|\Delta\varepsilon|$ values observed indicate that mhcpe promotes the binding of $V^{IV}O$ to HSA; it is probable that the binding takes place with $V^{IV}O$ bound to more than one protein residue, *e.g.* $N_{imidazole}$ atoms of His residues, $O_{carboxylate}$ atoms of Asp residues, or others.

Fig. SI-9-1† depicts CD spectra in the 200–250 nm range of a solution containing HSA, and of this after stepwise additions of a solution containing $V^{IV}OSO_4$ and mhcpe in a 1 : 2 molar ratio. Upon addition of this solution of $V^{IV}O(mhcpe)_2$ up to a molar ratio of 1 : 1 : 2 (HSA : $V^{IV}O$: mhcpe), the CD spectrum shows no change. Upon further additions of the $V^{IV}O(mhcpe)_2$ solution, the pattern of the CD spectra does not change, but the $|\Delta\varepsilon|$ values globally increase. As mhcpe and $V^{IV}O$–mhcpe complexes absorb in this wavelength range, ICD bands may be responsible for the increase in the $\Delta\varepsilon$ values. Thus, we cannot conclude with certainty that upon addition of a complex there are conformational changes of the protein; probably these changes take place but are not very extensive.

Interactions of vanadium–mhcpe complexes with hTF and HSA with concentrations close to those expected in blood plasma

In the UV region, namely in the 290–390 nm range, HSA has a negative band up to *ca.* 330 nm, and the $\Delta\varepsilon$ values are *ca.* zero for λ > 330 nm. Fig. 15 depicts the changes observed upon adding a solution containing $V^{IV}OSO_4$ and mhcpe (1 : 2 molar ratio) trying to simulate *in vivo* conditions, where it is likely that the concentration of $V^{IV}O$ or $V^{IV}O$-complexes will not be higher than 80 μM (possibly it will be lower, except for short periods if $V^{IV}O$-complexes are introduced by injection). The changes observed are significant, *i.e.* $V^{IV}O$–mhcpe complexes bind to HSA and this yields very small changes in the CD spectra in this wavelength range, namely at *ca.* 320–350 nm where mhcpe presents a relatively strong band (see Fig. 2).

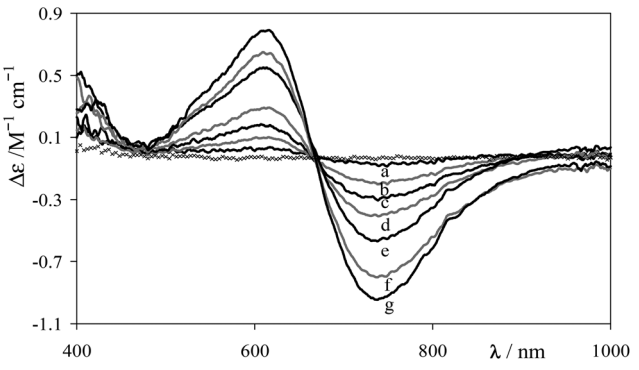

Fig. 14 CD spectra of HSA (0.650 mM) solution (dark grey) and after stepwise additions of a solution containing $V^{IV}OSO_4$ and mhcpe in a 1 : 1 molar ratio in Hepes-CL buffer at pH 7.4. The HSA : $V^{IV}OSO_4$: mhcpe molar ratios are as indicated: a: (1 : 0.5 : 0.5); b: (1 : 1 : 1); c: (1 : 1.5 : 1.5); d: (1 : 2 : 2); e: (1 : 3 : 3); f: (1 : 4 : 4); g: (1 : 5 : 5). The spectra were recorded with a 50 mm optical path quartz cell (section ESI-4†).

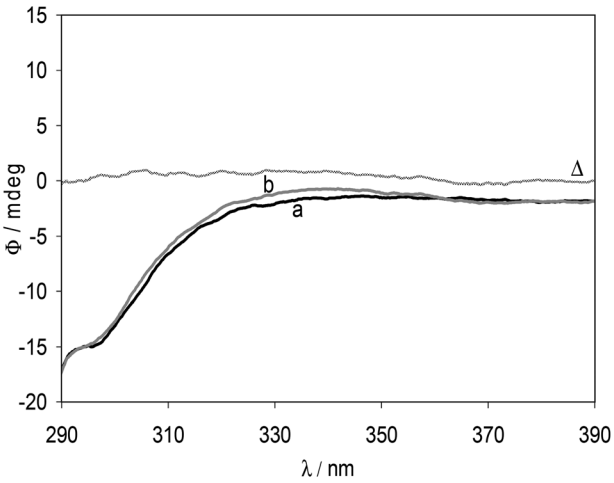

Fig. 15 CD spectra of (a) a solution containing HSA (0.630 mM), and (b) a solution containing HSA (0.630 mM), $V^{IV}OSO_4$ (80 μM) and mhcpe (160 μM) in Hepes-S buffer at pH 7.4. The spectra were recorded with a 2 mm optical path quartz cell. The change in signal in the range 310–350 nm from spectrum (a) to (b) is significant and is probably due to an induced CD band of the mhcpe ligand. The difference between the two spectra is the grey curve labelled with '△'.

Fig. 16A depicts CD spectra of solutions containing HSA and hTF in concentrations close to those present in human blood plasma. Spectrum (a) corresponds to the CD signal for the solution containing the two proteins, and (b–e) after stepwise additions of a solution containing $V^{IV}OSO_4$ and mhcpe in a 1 : 1 molar ratio. The spectra of Fig. 15 and 16A differ significantly and clearly indicate that hTF is the main $V^{IV}O$-binder, ternary (at least) hTF–$V^{IV}O$–mhcpe species being formed. In fact, comparing what is depicted in Fig. 15, 16A and 16B, the changes observed in Fig. 16A are indeed very similar to those observed in solutions only containing hTF and $V^{IV}OSO_4$, namely the clear observation of the strong ICD band of mhcpe with λ_{max} at *ca.* 330 nm. Quite similar observations were made with solutions containing HSA (0.630 mM) and hTF (40 μM) and adding $V^{IV}O(dhp)_2$ or $V^{IV}O(maltol)_2$ (see the section ESI-6†). For these simulated human blood plasma conditions, hTF is again the main $V^{IV}O$-binder, with ternary (at least) hTF–$V^{IV}O$–dhp or –maltol species also being formed.

Clearly, as in the case of the solutions containing amino acids or dipeptides (see above), the formation of ternary species HSA–$V^{IV}O$–mhcpe enhances the interaction of the metal ion with chiral groups of the protein, the intensity of the ICD bands due to V^{IV} d–d transitions increasing. Sanna

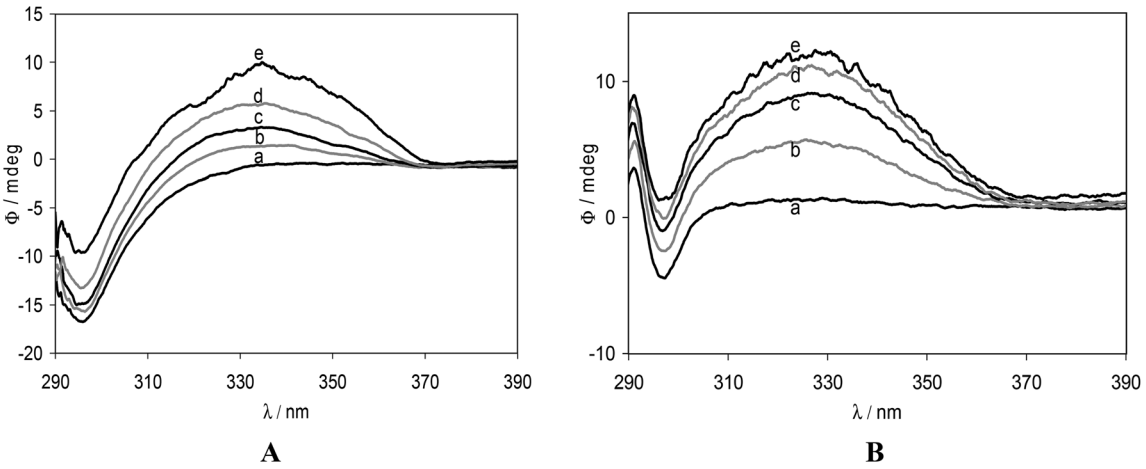

Fig. 16 CD spectra of (A) HSA–hTF–$V^{IV}O$–mhcpe solutions: a solution containing HSA (0.630 mM) and hTF (40 μM) (a) and after stepwise additions of a solution containing $V^{IV}OSO_4$ and mhcpe in a 1 : 1 molar ratio in Hepes-S buffer at pH 7.4: the concentrations are as indicated: (b) 630 μM HSA + 40 μM hTF + 40 μM $V^{IV}O(mhcpe)_2$; (c) 630 μM HSA + 40 μM hTF + 80 μM $V^{IV}O(mhcpe)_2$; (d) 630 μM HSA + 40 μM hTF + 160 μM $V^{IV}O(mhcpe)_2$; (e) 630 μM HSA + 40 μM hTF + 320 μM $V^{IV}O(mhcpe)_2$. (B) hTF–$V^{IV}O$–mhcpe solutions: (a) 100 μM hTF; (b) 100 μM hTF + 100 μM $V^{IV}O(mhcpe)_2$; (c) 100 μM hTF + 200 μM $V^{IV}O(mhcpe)_2$; (d) 100 μM hTF + 300 μM $V^{IV}O(mhcpe)_2$; (e) 100 μM hTF + 500 μM $V^{IV}O(mhcpe)_2$. The spectra were recorded with a 2 mm optical path quartz cell.

et al.,[46] in the case of dhp, suggested the formation of $V^{IV}O(dhp)_2$–HSA ternary species, with the $V^{IV}O$-unit bound to a histidine residue, and a similar species $V^{IV}O(maltol)_2$–HSA was predicted in the case of maltol. We cannot rule out the formation of the similar species $V^{IV}O(mhcpe)_2$–HSA in the present system; however, the CD spectra of Fig. 14 totally differ from those of solutions containing $V^{IV}OSO_4$ and histidine,[73] and from solutions containing $V^{IV}OSO_4$, histidine and mhcpe. The CD spectra also totally differ for the HSA and hTF systems, indicating that distinct species should be formed and not just $V^{IV}O(carrier)_2$–protein species.

Transport of vanadium–mhcpe complexes in blood

If the compound is taken orally, a significant amount of $V^{IV}O$–mhcpe complexes may be present at the pH of the stomach, as inferred from the obtained speciation diagram (Fig. 4), but presently it is not possible to anticipate if the $V^{IV}O$–mhcpe complexes will be extensively absorbed in the gastro-intestinal tract or not.

The models described indicate that when $V^{IV}O$–mhcpe complexes are introduced into the blood stream, the $V^{IV}O$ moiety will preferentially bind to hTF forming hTF–$V^{IV}O$–mhcpe complexes. However, thermodynamic models correspond to equilibrium conditions and these cannot be unambiguously applied to living systems. If only thermodynamic considerations are assumed, it may be anticipated that if a small amount of a solution containing $V^{IV}O$–mhcpe complexes is injected into blood, the metal ion is transported by hTF mainly as $(V^{IV}O)$(hTF)(mhcpe) and $(V^{IV}O)_2$(hTF)$(mhcpe)_2$ complexes.

Conclusions

A new pyrimidinone, mhcpe (HL), was synthesized, its structure determined by single crystal X-ray diffraction and its acid–base properties were studied by potentiometric and spectrophotometric methods, as well as by DFT calculations. The most stable structure for each of the H_2L^+, HL and L^- forms in aqueous solution was established, thus enabling the assignment of the groups involved in the protonation/deprotonation processes: a proton bound to a N-ring atom in the case of K_{a1} and an O-catecholate-type proton in the case of K_{a2}.

Aqueous solution studies regarding the identification and characterization of complexes formed by $V^{IV}O^{2+}$ and mhcpe were carried out in the pH range 2–11 using potentiometry, EPR and UV-Vis techniques. An equilibrium model was established as well as the binding modes corresponding to each stoichiometry. The $mhcpe^-$ ligand forms quite stable complexes with $V^{IV}O^{2+}$, the global binding ability being similar to that of $maltol^-$ and lower than that of dhp^-. The possibility of formation of ternary complexes $V^{IV}O$–mhcpe-L′ with several amino acids was confirmed.

The interaction of V–mhcpe complexes with human plasma proteins (transferrin and albumin) was evaluated. In the case of transferrin the mhcpe ligand is involved in the binding of $V^{IV}O^{2+}$ to the protein, the most important species formed corresponding to $(V^{IV}O)$(hTF)(mhcpe) and $(V^{IV}O)_2$(hTF)$(mhcpe)_2$. Strong induced CD-signals were recorded for mhcpe-intraligand CD bands as well as ICD in d–d transitions of V^{IV}, indicating that these V^{IV}–mhcpe ternary species are in close interaction with chiral groups of the iron binding site of hTF; similar bands were also recorded for $(V^{IV}O)_n$(hTF)$(maltol)_m$ and $(V^{IV}O)_n$(hTF)$(dhp)_m$ ternary complexes.[57]

$V^{IV}O$–HSA–mhcpe species may also form and were identified by both EPR and CD spectra. However, CD spectra recorded under conditions close to those existing in human blood serum, namely with a concentration of HSA of *ca.* 630 μM and hTF of *ca.* 40 μM, up to a total vanadium concentration of 80 μM, indicate that $V^{IV}O$–mhcpe species bind

mainly to hTF. Similar conclusions are made in the case of maltol and dhp. For higher vanadium concentrations HSA may start being a relevant $V^{IV}O$-binder.

When Fe^{III} is present or is added to solutions containing hTF, $V^{IV}O^{2+}$ and mhcpe, the Fe^{III} binds hTF removing an equivalent number of $V^{IV}O$-complexes, and EPR spectra clearly show both the signals of Fe^{III}–hTF and of $V^{IV}O$–hTF species. However, in the presence of Fe^{III} the EPR and CD spectroscopic signals due to $V^{IV}O$ disappear much faster than in its absence, and a significant amount of V^{V}–hTF species is detected by ^{51}V NMR in the obtained solutions.

In conclusion, the newly synthesized compound mhcpe is a suitable carrier ligand for $V^{IV}O$, being able to engage the metal ion in stable complexes and assisting its transport in blood plasma conditions through transferrin binding with the formation of ternary species involving the $V^{IV}O$ metal ion, mhcpe and transferrin. Binding to mhcpe does not modify the preference of $V^{IV}O^{2+}$ for transferrin despite the major concentration of albumin available in blood plasma conditions. These interactions may be of relevance for the cellular uptake of $V^{IV}O$ mediated by the transferrin receptor.

Experimental section

Synthesis

Synthesis of benzyl benzyloxyacetate.[80] A suspension of sodium hydride (1.18 g, 60% in oil, 30 mmol) in dry THF (20 mL) was added to benzyl alcohol (3 g, 30 mmol) at 0 °C. Benzyl bromoacetate (6.9 g, 30 mmol) was added dropwise. After being stirred for 24 hours, the reaction mixture was poured into water and extracted twice with ether. The combined organic extracts were dried over anhydrous Na_2SO_4/H_2SO_4 (conc.). Purification on a silica gel column (hexane–ethyl acetate 6 : 1) yielded the title compound as an oil. Yield: 76%. ^1H NMR ($CDCl_3$, δ): 7.38 (m, 10H, Ph); 5.22 (s, 2H, Ph-CH_2-OCO); 4.65 (s, 2H, Ph-CH_2-OCH_2); 4.16 (s, 2H, OCO-CH_2-O).

Synthesis of 2-methyl-3*H*-5-benzyloxy-6-carboxy-4-pyrimidinone ethyl ester. (Adapted from ref. 41.) Benzyl-2-(benzyloxy)-acetate (14.13 g, 55.13 mmol), diethyloxalate (8.06 g, 55.13 mmol), and ethanol (0.2 mL) were dissolved in dry THF (100 mL). NaH (2.34 g, 60% in oil, 58.5 mmol) was added and the mixture was stirred at room temperature for 48 h. THF was removed under vacuum, and the residue was dissolved in ethanol (100 mL), followed by addition of sodium ethoxide (3.75 g, 55.1 mmol) and acetamidine hydrochloride (5.21 g, 5.11 mmol). After stirring at 60 °C for 14 h, the resulting suspension was cooled to room temperature, and most of the solvent removed under vacuum. The resulting oil was extracted with CH_2Cl_2 and H_2O. The pH of the aqueous phase was adjusted to ~6 with HCl (conc.) and both phases were washed several times. The organic phase was separated, dried with anhydrous Na_2SO_4 and the CH_2Cl_2 evaporated till an orange oil was obtained. This was immediately shaken with diethyl ether (30 mL) and left in the freezer. A white solid precipitated, filtered, and 4.3 g of 2-methyl-3*H*-5-benzyloxy-6-carboxy-4-pyrimidinone ethyl ester were obtained. The residual oil was separated by chromatography (silica gel) with a mixture of ethyl acetate and CH_2Cl_2 (1 : 1) and 2.1 g 2-methyl-3*H*-5-benzyloxy-6-carboxy-4-pyrimidinone ethyl ester were additionally obtained. Yield: 40.5%. M.p.: 125–126 °C. Elemental analysis: found (calc. for $C_{15}H_{16}N_2O_4$): C, 62.5 (62.5); H, 5.6 (5.6); N, 9.7 (9.7). Mass spectrometry (FAB-MS^+, thioglycerol matrix): 289 amu $[C_{15}H_{17}N_2O_4]^+$. ^1H NMR ($CDCl_3$, 200 MHz, 293 K, δ): 12.84 (br s, 1H, amide NH), 7.46 (m, 2H, Ph), 7.37 (m, 3H, Ph), 5.28 (s, 2H, CH_2-Ph), 4.37 (q, 2H, J = 7.1 Hz, OCH_2), 2.51 (s, 3H, 2-Me), 1.34 (t, 3H, J = 7.1 Hz, CH_2-Me).

Synthesis of 2-methyl-3*H*-5-hydroxy-6-carboxy-4-pyrimidinone ethyl ester (1, mhcpe). The 2-methyl-3*H*-5-benzyloxy-6-carboxy-4-pyrimidinone ethyl ester (0.600 g, 2.08 mmol) was dissolved in acetic acid (20 mL) and Pd/C 5% (30 mg) was added to the solution. This mixture was stirred vigorously under a H_2 atmosphere for 8 h at room temperature. After Pd/C filtration, a precipitate was obtained from the solution by partial evaporation of the solvent. This precipitate was dissolved in methanol. The white solid obtained from this methanolic solution is **mhcpe**, **1**, (0.22 g; yield: 53.4%). Crystals from the solution suitable for X-ray diffraction were obtained. Elementary analysis: found (calc. for $C_8H_{10}N_2O_4$): C, 48.2 (48.5); H, 5.0 (5.1); N, 14.0 (14.1). M.p.: 220–222 °C. Mass spectrometry (FAB-MS^+, 3-NOBA matrix): 199 amu. $[C_8H_{11}N_2O_4]^+$. ^1H NMR ($CDCl_3$, 200 MHz, 293 K, δ): 12.76 (br s, 1H, amide NH), 10.82 (br s, 1H, OH), 4.52 (q, 2H, J = 7.3 Hz, O-CH_2-Me), 2.51 (s, 3H, 2-Me), 1.46 (t, 3H, J = 7.1 Hz, ester CH_3); ^{13}C NMR ($CDCl_3$, 500 MHz, 293 K, δ): 169.7 (***C***OOEt), 160.5 (pyrimidinone *N*-***C***-2-Me-N), 149.2 (pyrimidinone ***C***=O), 148.2 (pyrimidinone ***C***-OH), 127.5 (pyrimidinone *N*-***C***-COH), 63.3 (O-***C***H_2-Me), 21.5 (pyrimidinone 2-Me), 14.2 (ester group ***C***H_3).

Synthesis of 2,3-dimethyl 5-benzyloxy-6-carboxy-4-pyrimidinone ethyl ester (2, dbcpe). A solution of **1** (4.88 g, 16.9 mmol) in DMF (20 mL) was added dropwise to a stirred suspension of NaH (0.745 g, 60% in oil, 18.6 mmol) in dry DMF (20 mL) over ~20 min maintaining gentle effervescence. After H_2 evolution had ceased, methyl iodide (1.27 mL, 20.4 mmol) was added in one portion and the reaction mixture was stirred at room temperature during 4 h. The excess hydride was quenched with ethanol (2 mL), and DMF was removed by rotary evaporation under vacuum. Addition of water produced an oily 'solid' which became an off-white crystalline mass upon further shaking. This solid was separated by filtration, dried briefly, and then washed with hexane (3 × 20 mL) to afford 3.0 g (~10 mmol) of crude 2,3-dimethyl-5-benzyloxy-6-carboxy-4-pyrimidinone ethyl ester (**2**, dbcpe). This crude product was recrystallized in chloroform and crystals of dbcpe suitable for X-ray diffraction were obtained. Yield: 58.8%. ^1H NMR ($CDCl_3$, 200 MHz, 293 K, δ): 7.47–7.33 (m, 5H, Ph), 5.25 (s, 2H, CH_2-Ph), 4.34 (q, 2H, J = 7.1 Hz, O-CH_2), 3.56 (s, 3H, 3-NMe), 1.32 (t, 3H, J = 7.1 Hz, CH_2-Me).

Synthesis of 2,3-dimethyl-5-benzyloxy-6-carboxy-4-pyrimidinone (4, HOPY acid). (Adapted from ref. 41.) ~3.0 g of

dbcpe and KOH (0.666 g; 11.8 mmol) were dissolved in methanol (50 mL) and stirred at room temperature. After 6 h the hydrolysis was complete, and a fine yellow-white precipitate had formed. After evaporation of the solvent the residue was dissolved in water (20 mL), filtered and slowly acidified with concentrated HCl. At pH ~ 4 a small amount of yellow precipitate was separated. At pH ~ 2 a white precipitate was isolated by filtration and washed with water. After drying under vacuum, 2.6 g of 2,3-dimethyl-5-benzyloxy-6-carboxy-4-pyrimidinone (**4**, HOPY acid; yield: 95.6%) were obtained. Elemental analysis: found (calc. for $C_{14}H_{14}N_2O_4$): C, 61.3 (61.5); H, 5.1 (5.1); N, 10.3 (10.2). M.p.: 179–180 °C. ^{1}H NMR ($CDCl_3$, 200 MHz, 293 K, δ): 7.53 (m, 3H, Ph), 7.36 (m, 2H, Ph), 5.49 (s, 2H, CH_2-Ph), 3.57 (s, 3H, 3-NMe), 2.56 (s, 3H, 2-Me).

Synthesis of *N*-methyl-2,3-dimethyl-5-benzyloxy-6-carboxy-amido-4-pyrimidinone. Carbonyl diimidazole (0.625 g, 3.86 mmol) was added in several portions during 10 min to a slurry of HOPY acid (**4**, 1 g, 3.63 mmol) in CH_2Cl_2 (10 mL). After a further 5 min period, methylamine (0.113 g, 1.82 mL of 2 M THF solution, 3.63 mmol) mixed with 5 mL of CH_2Cl_2 was added dropwise during 5 min, and the reaction mixture was stirred for 12 h. The CH_2Cl_2 was removed and the resultant oil shaken with ethanol–diethyl ether (1 : 10). The white precipitate obtained was filtered and washed with diethyl ether. Yield, 51.8%. Elemental analysis: found (calc. for $C_{15}H_{17}N_3O_3$): C, 62.9 (62.7); H, 6.0 (6.0); N, 15.1 (14.6). M.p.: 62–63 °C. Mass spectrometry (FAB-MS$^+$, 3-NOBA matrix): 288 amu $[C_{15}H_{18}N_3O_3]^+$. ^{1}H NMR ($CDCl_3$, 200 MHz, 293 K, δ): δ 7.74–7.33 (m, 5H, Ph), 7.09 (s, 1H, NH-amide), 5.28 (s, 2H, CH_2-Ph), 3.57 (s, 3H, 3-NMe), 2.88 (d, 3H, J = 4.9 Hz, NH-Me), 2.54 (s, 3H, 2-Me); ^{13}C NMR ($CDCl_3$, 500 MHz, 293 K, δ): 163.4 (***C***ONH), 160.5 (pyrimidinone *N*-***C***-2-Me-N), 153.3 (pyrimidinone ***C***=O), 142.1 (pyrimidinone ***C***-amide), 140.5 (Ph group CH_2-***C***), 136.3 (N***C***C=O), 129.0–128.6 (5C, Ph), 74.9 (O-***C***H_2-Ph), 31.8 (1C, 3-NMe), 23.2 (pyrimidinone 2-Me).

Synthesis of *N*-methyl-2,3-dimethyl-5-hydroxy-6-carboxy-amido-4-pyrimidinone (*N*-MeHOPY, 3). *N*-Methyl-2,3-dimethyl-5-benzyloxy-6-carboxyamido-4-pyrimidinone (0.500 g, 1.74 mmol) was dissolved in acetic acid (20 mL) and Pd/C 5% (30 mg) was added to the solution. This mixture was stirred vigorously under a H_2 atmosphere for 4 h at room temperature. After Pd/C filtration, an oil was obtained from the solution by partial evaporation of the solvent and was precipitated with hexane. A white precipitate of *N*-MeHOPY (**3**) was isolated by filtration and was washed with hexane. Crystals of *N*-MeHOPY suitable for X-ray diffraction were grown in acetic acid–hexane (1 : 4) solution at low temperature. Yield: 32.0%. Elemental analysis: found (calc. for $C_8H_{11}N_3O_3$): C, 48.9 (48.7); H, 5.8 (5.6); N, 21.8 (21.3). M.p.: 163–164 °C. Mass spectrometry (FAB-MS$^+$, 3-NOBA matrix): 198 amu $[C_8H_{12}N_3O_3]^+$. ^{1}H NMR ($CDCl_3$, 200 MHz, 293 K, δ): 12.03 (br s, 1H, OH), 7.65 (br s, 1H, NH amide), 3.56 (s, 3H, 3-NMe), 3.0 (d, 3H, J = 4.9 Hz, NH-Me), 2.46 (s, 3H, 2-Me); ^{13}C NMR ($CDCl_3$, 500 MHz, 293 K, δ): 168.2 (***C***ONH), 158.8 (pyrimidinone *N*-***C***-2-Me-N), 148.0 (pyrimidinone ***C***-amide), 146.5 (pyrimidinone ***C***=O), 125.37 (pyrimidinone ***C***-OH), 31.8 (3-NMe), 25.7 (NH-Me), 22.7 (pyrimidinone 2-Me).

Determination of protonation and formation constants of mhcpe and $V^{IV}O$–mhcpe systems

pH-potentiometric titrations. All measurements were made in aqueous solution. The purity of the ligand was checked pH-potentiometrically and the exact concentrations of solutions were determined by checking the inflection points of the titrations by the Gran method. Two stock solutions of $V^{IV}O(ClO_4)_2$ were used and their $V^{IV}O^{2+}$ and H_3O^+ concentrations were determined and standardized as reported earlier[62,81] by pH-potentiometry. The $V^{IV}O^{2+}$ concentrations were *ca.* 300 mM and *ca.* 180 mM and dilutions were made as appropriate. The V^V stock solution (~30 mM) was prepared by dissolving KVO_3 (Sigma-Aldrich) in an accurately measured volume of a KOH solution of known molarity (0.2034 M), and its OH^- concentration was calculated taking into account the total volume of the vanadate stock solution prepared.

All solutions were manipulated in an inert atmosphere (high purity N_2). The ionic strength was adjusted to 0.20 M KCl and the temperature was 25.0 ± 0.1 °C. The pH was measured with a Thermo Orion 420A+ pH-meter with a Mettler Toledo U402-M3-S7/200 combined electrode, calibrated for hydrogen ion concentration as described earlier.[62] The ionic product of water was pK_w = 13.72.

Determination of protonation constants. For the determination of the protonation constants several sets of UV absorption spectra (210–380 nm) with concentrations of *ca.* 10^{-4} M were measured in the pH range *ca.* 0.5 to 12, and five pH titration curves were also measured in the pH range *ca.* 1.8 to 12. An individual calibration curve EMF *vs.* $[H^+]$ was established for pH values < ~2, valid for the present medium and electrodes. For this purpose a set of HCl solutions were prepared with known H^+ concentration, from pH *ca.* 0.8 to 2.0, all with an ionic strength of 0.20 M. The protonation constant β_2 of mhcpe was determined from the five titration curves of 10 to 15 mL samples, with initial concentrations in the range 0.0032 to 0.012 M, using the SUPERQUAD computer program.[82] Both protonation constants β_1 and β_2 of MHCPE were determined from the UV spectra in the pH range 0.8 to 8 using the PSEQUAD computer program.[59] The calculated pK_a values determined from the UV spectra were pK_{a1} = 1.14 and pK_{a2} = 6.34. The pK_{a2} calculated from the pH-metric titration is 6.36.

Determination of formation constants. For the determination of the stability constants of the $V^{IV}O$–mhcpe system several sets of visible absorption spectra (350–900 nm) were measured in the pH range *ca.* 0.7 to 12: (i) C_{VO} ~ 0.003 M and L : M = 1.77 (from pH 2.5 to 8.0 and pH ~ 11.8); (ii) C_{VO} ~ 0.005 M and L : M = 2.76 (from pH 0.98 to 9.9); (iii) C_{VO} ~ 0.006 M and L : M = 3.05 (from pH 1.8 to 8.4); (iv) C_{VO} ~ 0.009 M and L : M = 1.41 (from pH 2.1 to 8.8); (v) at pH ~ 7.2 from C_{VO} ~ 0.0027 to ~ 0.0091 M with C_{MHCPE} ~ 0.0182 M. Several pH-metric titrations were also carried out with 12.0 mL samples with total oxovanadium(IV) concentrations in the range 0.002–0.0055 M, and L : M ratios from 1.0 to 4.6.

These titrations were normally done from pH 1.8 up to 10, unless very extensive hydrolysis or very slow equilibration was detected (this only for L : M = 1.0, for pH ≥ 4.0), with a KOH solution of known concentration (*ca.* 0.2 M) under a N_2 atmosphere in thermostatized cells. The stock $V^{IV}O(ClO_4)_2$ solutions used were the same as for the spectrophotometric titrations.

The concentration stability constants $\beta_{pqr} = [M_pL_qH_r]/[M]^p[L]^q[H]^r$ were calculated using the SUPERQUAD[82] and the PSEQUAD[59] computer programs. The formation of the following $V^{IV}O$–hydroxo complexes was taken into account: $[V^{IV}O(OH)]^+$, $[(V^{IV}O)_2(OH)_2]^{2+}$, $[(V^{IV}O)_2(OH)_5]^-$ and $[V^{IV}O(OH)_3]^-$. As is discussed in ref. 61 and 62 the log β of $[(V^{IV}O)_2(OH)_5]^-$ and $[V^{IV}O(OH)_3]^-$ are not known accurately; thus the calculations for pH > 4 may not be entirely reliable, particularly for systems and experimental conditions where these $V^{IV}O$–hydroxo complexes have significant concentrations.

Conditional stability constants of apo-hTF–$V^{IV}O$–mhcpe species at pH 7.4. For all experiments a stock $V^{IV}O(SO_4)$ solution was used (*ca.* 100 mM), which was diluted as appropriate. The conditional formation constants calculated for the $V^{IV}O$–apo-hTF system[40] using the PSEQUAD computer program are: log K_1 = log β_1 = 13.4 and log K_2 = 11.9 (log β_2 = 25.3) and correspond to the reactions at pH 7.4 (n = 1 or 2):

$$n V^{IV}O^{2+} + \text{apo-hTF}^{\text{protonation state at pH} = 7.4} \rightleftarrows (V^{IV}O)_n\text{–hTF}$$

The hydrolytic constants of $V^{IV}O^{2+}$ (see above) were taken into account in the calculations.

The conditional formation constants K_{pqr} calculated for the $V^{IV}O$–apo-hTF–mhcpe system correspond to the reactions at pH 7.4 (p,r = 1 or 2, q = 1):

$$p V^{IV}O^{2+} + q\ \text{apo-hTF}^{\text{protonation state at pH} = 7.4} + r\ \text{mhcpe}^- \rightleftarrows (V^{IV}O)_p(\text{hTF})_q(\text{mhcpe})_r$$

The hydrolytic constants of $V^{IV}O^{2+}$, the protonation constants of mhcpe$^-$, all formation constants of $V^{IV}O$–mhcpe complexes (see above) and the conditional stability constants for the binary species $(V^{IV}O)$–hTF and $(V^{IV}O)_2$–hTF[40] were taken into account in the calculations for the $V^{IV}O$–apo-hTF–mhcpe system with the PSEQUAD computer program.

Spectroscopic measurements

Physical and spectroscopic studies. IR spectra were recorded either with a BioRad FTS 3000 MX FTIR or with a Jasco FTIR 430 spectrometer. The CD spectra were recorded with a JASCO 720 spectropolarimeter, either with a red-sensitive photomultiplier (EXEL-308) suitable for the 400–1000 nm range or with the photomultiplier suitable for the 170–700 nm range. Visible spectra were recorded with a Hitachi U-2000 spectrophotometer. The EPR spectra were recorded at 77 K (on glasses made by freezing solutions in liquid nitrogen) with a Bruker ESP 300E X-band spectrometer. The ^{1}H NMR and ^{51}V NMR spectra were obtained on a Bruker Avance III 400 MHz spectrometer at *ca.* 25 °C.

UV-Vis spectroscopy. All measurements with the mhcpe solutions were made in water at I = 0.20 M KCl (for pH < 2 KCl–HCl mixtures with I = 0.2 M were used, see below). The temperature was kept at 25.0 ± 0.3 °C with circulating water. Unless otherwise stated, by visible (Vis) spectra we mean a representation of ε_m *vs.* λ [ε_m = absorption/(bC_M), where b = optical path and C_M = total V^{IV} concentration]. The spectral range covered was normally 210–390 nm (UV) or 350–900 nm (Vis), with a 10 mm optical path quartz cell. Normally, but not in all cases, the spectra were recorded changing the pH with approximately fixed total vanadium and ligand concentrations.

Circular dichroism. All measurements were made in water and the temperature was kept at *ca.* 25.0 ± 1 °C. Unless otherwise stated, by circular dichroism (CD) spectra we mean a representation of $\Delta\varepsilon$ values *vs.* λ [$\Delta\varepsilon$: differential absorption/(bC_P) and C_P = total protein concentration]. The spectral range covered was either 190–250 nm (1 mm optical path) or 250–400 nm (2 or 10 mm optical path) or 400–1000 nm (10 or 50 mm optical path, section ESI-4†). All measurements and operations of the spectropolarimeter were computer-controlled, and the sample compartment was continuously flushed with nitrogen gas.

EPR spectroscopy. In the absence of ethylene glycol or DMSO a relatively broad background was present in most of the frozen solution EPR spectra, therefore most spectra of solutions containing $V^{IV}O^{2+}$ and mhcpe were run with aqueous solutions containing 5% DMSO to promote the formation of a good glass.

Several sets of EPR spectra were measured for the $V^{IV}O$–mhcpe system in the pH range *ca.* 0.7 to 12: (i) $C_{VO} \sim 0.004$ M and L : M = 4.02 (from pH 7.4 to 11.3); (ii) $C_{VO} \sim 0.005$ M and L : M = 2.76 (from pH 0.98 to 9.9); (iii) $C_{VO} \sim 0.006$ M and L : M = 3.05 (from pH 1.8 to 8.4); (iv) $C_{VO} \sim 0.007$ M and L : M = 1.53 (from pH 7.6 to 11.0); (v) $C_{VO} \sim 0.009$ M and L : M = 1.41 (from pH 2.1 to 8.8); (vi) at pH ~ 7.2 from $C_{VO} \sim 0.0027$ to ~ 0.0091 M with $C_{mhcpe} \sim 0.0182$ M.

The EPR spectra help to elucidate which groups coordinate in solution. For the $V^{IV}O$-systems we used the additivity rule to estimate the hyperfine coupling constant A_z^{est} (see above). To calculate the relevant spin-Hamiltonian parameters from the experimental EPR spectra, these were either simulated using a program from Rockenbauer and Korecz,[63] or an iterative procedure developed by Chasteen *et al.*[66] using the corrected equations of Casella *et al.*[83] was used.

^{1}H and ^{51}V NMR spectroscopy. All samples were prepared at room temperature immediately before the acquisition of the NMR spectra. Ligand solutions for the ^{1}H NMR pH titrations were prepared in D_2O (99.995%D) weighting the appropriate amount of the ligand in order to have the desired concentration. When relevant the pD values of these solutions were adjusted with DCl and CO_2-free NaOD solutions, and measured either on a Crison MicropH 2002 pH-meter with an Ingold 405-M5 combined electrode, or using a Thermo Orion 420A+ pH meter with a Mettler Toledo U402-M3-S7/200 combined microelectrode (all calibrated at 20 ± 1 °C with standard

aqueous buffers at pH 4.0 and 7.0). The final values of pD were determined from pD = pH* + 0.40, where pH* corresponds to the reading of the pH meter.

For the acquisition of ^{1}H NMR spectra to access protonation steps of mhcpe a ~5 mM solution of mhcpe was prepared at pD ~ 10 in D_2O, by addition of CO_2-free NaOD. The measurements were done down to pH 1 by addition of DCl (or NaOD, whenever necessary).

The ^{1}H and ^{51}V NMR chemical shifts were referenced relative to DSS (sodium 3-trimethyl-silyl-d_4-propionate) at 0 ppm and to external neat $VOCl_3$ at 0 ppm, respectively. ^{51}V NMR acquisition parameters were: 33 kHz spectral width, 30 μs pulse width, 1 s acquisition time and 10 Hz line broadening. The signal intensities of the NMR resonances were obtained using the line-fitting routine supplied with the NUTS™ PC-based NMR spectral analysis program.

Preparation of solutions containing vanadium, apo-transferrin, mhcpe and iron

Most samples containing $V^{IV}O$ were manipulated in a glove bag purged with nitrogen or argon gas.

Hepes-S buffer. The composition of the Hepes-S buffer used is 50 mM Hepes (Sigma-Aldrich), 25 mM carbonate added as $NaHCO_3$ (Sigma-Aldrich), 1 mM phosphate added as $NaH_2PO_4{\cdot}H_2O$ (Merck) and 0.20 mM KCl (Merck). This buffer system was adjusted to a pH of 7.4 using conc. KOH.

Hepes-CL buffer. The composition of the Hepes-CL buffer used is similar to that of Hepes-S, but additionally it also contains: 0.1 mM citrate and 1.5 mM lactate. This buffer system was also adjusted to pH 7.4 using conc. KOH. No clearly measurable CD spectrum in the visible range (400–1000 nm) is obtained with solutions of $V^{IV}OSO_4$ and mhcpe (1 : 1) in this buffer; thus no ternary $V^{IV}O$–lactate–mhcpe or $V^{IV}O$–citrate–mhcpe complexes can be detected by CD under these conditions.

PBS buffer. Phosphate buffered saline (PBS) from Sigma-Aldrich was used. One tablet dissolved in 200 mL of Millipore® water yields 0.01 M phosphate buffer, 0.0027 M potassium chloride and 0.137 M sodium chloride, pH 7.4, at 25 °C. Every PBS solution used in this work also contains 25 mM $NaHCO_3$.

$V^{IV}O$-solutions. For all experiments involving studies with solutions containing serum proteins, a stock $V^{IV}O(SO_4)$ solution was used (99.0 mM, pH ~ 2), which was first diluted as appropriate (*e.g.* to 9.90 mM or 0.990 mM), and then used in the experiments.

Protein solutions. Human apo-transferrin solutions were prepared by dissolving the protein, either transferrin (Sigma, T4382) or human serum albumin (Sigma, A1653, fatted) in buffer at pH 7.4. The solutions were allowed to stand for at least 1 h to allow equilibration. During this period they were gently swirled without strong agitation. The concentrations of the protein solutions were determined by measuring the absorbance at 280 nm using an extinction coefficient of 92 300 M^{-1} cm^{-1} for apo-transferrin,[40,84,85] and 36 850 M^{-1} cm^{-1} for HSA.[86,87] Normally argon was bubbled through all solutions prior to use for measurements with V^{IV}-complexes to displace any oxygen that may be present, and the solutions were kept and manipulated under an argon atmosphere inside a glove bag.

Iron transferrin solutions were prepared by dissolving the ferrous ammonium sulfate hexahydrate salt ($Fe(NH_4)_2(SO_4)_2{\cdot}6H_2O$, Mohr's salt) in the apo-hTF solution in buffer. The solution of Fe–hTF was kept for *ca.* 24 h so that Fe^{III} forms and binds to hTF yielding the Fe^{III}–hTF complex. For $(Fe)_2$–hTF an extinction coefficient of 113 000 M^{-1} cm^{-1} was used.[51]

Loading of Fe^{III} onto hTF. Samples containing Fe^{III} were prepared from stock solutions of Mohr's salt ($(NH_4)_2Fe(SO_4)_2{\cdot}6H_2O$). Normally to form holo-transferrin (orange solution), to saturate apo-transferrin with iron, apo-transferrin solutions (colourless solution) were mixed with ferrous ammonium sulfate hexahydrate in Hepes-S or Hepes-CL buffer pH 7.4. The Fe^{II}, from the stock solution, is then rapidly oxidized to Fe^{III} in the presence of the protein and after degassing the solution. $FeCl_3$ (Merck) was used in some cases to prepare solutions that were added to solutions containing apo-hTF and/or $V^{IV}OSO_4$.

Several sets of CD (visible range) and EPR spectra were measured for the $V^{IV}O$–apo-hTF–mhcpe system, normally with a transferrin concentration of 750 μM and varying the $V^{IV}O$- and mhcpe-concentration. 750 μM was an adequate $V^{IV}O$ concentration (and thus hTF concentration for 1 : 1 ratios) to produce EPR spectra suitable for simulation. Most of these spectra were measured with buffer solutions at pH = 7.4. Most preparations were done under argon doing all manipulations inside glove bags. The CD spectra were run either with 10 mm or 50 mm optical path quartz cells (see ESI-4†) in the wavelength range 400–1000 nm, and the sample compartment was continuously flushed with nitrogen gas. Several CD spectra were measured with human serum albumin (*ca.* 0.63 mM, the HSA blood plasma concentration) varying the $V^{IV}O$- and mhcpe-concentration.

Several sets of CD spectra (UV range) were measured for the $V^{IV}O$–apo-hTF–mhcpe system, normally with a apo-transferrin concentration of 100 μM and varying the $V^{IV}O$- and mhcpe-concentration, either using a 2 mm or a 10 mm optical path quartz cells in the wavelength range 250–400 nm.

A few CD spectra (far-UV range) were measured for the $V^{IV}O$–apo-hTF, $V^{IV}O$–albumin and $V^{IV}O$–albumin–mhcpe systems, normally with a protein concentration of *ca.* 5–10 μM and varying the $V^{IV}O$ or the $V^{IV}O$–mhcpe concentration (section ESI-9†), using a 1 mm optical path quartz cell in the wavelength range 190–250 nm.

Several sets of CD spectra (UV range) were measured for the $V^{IV}O$–apo-hTF–HSA–mhcpe system, with an albumin concentration of 630 μM and a transferrin concentration of 40 μM and varying the $V^{IV}O$- and mhcpe-concentration. These spectra were measured with Hepes-S buffer solutions at pH = 7.4 and the preparations were done under argon doing all manipulations inside glove bags. The CD spectra were run with a 2 mm optical path quartz cell in the wavelength range 250–400 nm,

and the sample compartment was continuously flushed with nitrogen gas.

X-ray crystal structure determinations

Three-dimensional X-ray data were collected on a Bruker SMART 1000 CCD diffractometer using a graphite monochromator and Mo-K_α radiation (λ = 0.71073 Å) by the ϕ–ω scan method (Table 6). Data were collected at room temperature. Reflections were measured from a hemisphere of data collected of frames each covering 0.3 degrees in ω. Of the 4415 for **1**, 8387 for **2** and 5823 for **3** reflections measured, all of which were corrected for Lorentz and polarization effects, and for absorption by semi-empirical methods based on symmetry-equivalent and repeated reflections, 985 for **1**, 1502 for **2** and 1870 for **3** independent reflections exceeded the significance level $|F|/\sigma(|F|) > 4.0$. Complex scattering factors were taken from the program package SHELXTL.[88,89] The structure was solved by direct methods and refined by full-matrix least-squares methods on F^2. In **1**, the hydrogen atoms were included in calculated positions and refined in riding mode except the hydrogen atom H(2O), which was located in the difference Fourier map and freely refined; in **2**, all of them were included in calculated positions; in **3** all of them were located in the difference Fourier map and freely refined. Refinement converged with allowance for thermal anisotropy of all non-hydrogen atoms. A weighting scheme $w = 1/[\sigma^2(F_o^2) + (0.113100P)^2]$ for **1**, $w = 1/[\sigma^2(F_o^2) + (0.108600P)^2 + 0.019500P]$ for **2** and $w = 1/[\sigma^2(F_o^2) + (0.056900P)^2 + 0.867500P]$ for **3**, where $P = (|F_o|^2 + 2|F_c|^2)/3$, were used in the later stages of refinement. A final difference Fourier map showed no residual density outside: 0.305 and −0.298 e Å^{-3} in **1**, 0.222 and −0.236 e Å^{-3} in **2**, 0.340 and −0.176 e Å^{-3} in **3**. CCDC 926545, 926546 and 926547 contain the supplementary crystallographic data for the structures reported in this paper.

Table 6 Crystal and structure refinement data[a] for mhcpe (**1**), dbcpe (**2**) and (dbcpe) and *N*-MeHOPY (**3**).

	1	2	3
Formula	$C_8H_{10}N_2O_4$	$C_{16}H_{18}N_2O_4$	$C_8H_{11}N_3O_3$
M_r	198.18	302.32	197.20
T [K]	298(2)	298(2)	298(2)
λ, Å [Mo, Kα]	0.71073	0.71073	0.71073
Crystal system	Monoclinic	Monoclinic	Monoclinic
Space group	$C2/c$	$P2_1/c$	$C2/c$
a [Å]	26.412(19)	10.6417(19)	16.600(2)
b [Å]	4.442(3)	8.0586(15)	7.8212(11)
c [Å]	15.994(11)	18.579(3)	14.414(2)
β [°]	113.034(12)	96.853(4)	105.112(2)
Z	8	4	8
V [Å3]	1727(2)	1581.9(5)	1806.7(4)
$D_{calc.}$ [g cm^{-3}]	1.525	1.269	1.450
μ [mm^{-1}]	0.124	0.092	0.113
Reflections measured	4415	8387	5823
Independent reflections[b]	985	1502	1870
R_{int}	0.0585	0.0377	0.0209
Goodness-of-fit on F^2	0.937	1.042	1.050
R_1[c]	0.0562	0.0564	0.0402
wR_2 (all data)[c]	0.1892	0.2078	0.1110

[a] The structure was solved using the SHELXS Program for Crystal Structure Determination and refined with the SHELXL Program for Crystal Structure Refinement.[89] [b] $I > 2\sigma(I)$. [c] $R_1 = \Sigma||F_o| - |F_c||/\Sigma|F_o|$, $wR_2 = \{\Sigma[w(|F_o|^2 - |F_c|^2)^2]/\Sigma[w(F_o^4)]\}^{1/2}$.

DFT computational details. All calculations were carried out using the GAUSSIAN 03 software package,[90] and the PBE1PBE functional, without symmetry constraints. That functional uses a hybrid generalised gradient approximation (GGA), including a 25% mixture of Hartree–Fock[91] exchange with DFT[60] exchange–correlation, given by Perdew, Burke and Ernzerhof functional (PBE).[92,93] The optimised geometries were obtained with a standard 6-31G(d,p)[94–98] basis set. A Natural Population Analysis (NPA)[99–104] and the resulting Wiberg indices[105] were used to study the electronic structure and bonding of the optimised species. The energy differences reported in Scheme 3 result from single point energy calculations using a 6-311++G(d,p)[106–110] basis set and the geometries optimised at the PBE1PBE/6-31G(d,p) level. Solvent (water) effects were considered in the energy calculations, using the Polarizable Continuum Model (PCM) initially devised by Tomasi and coworkers[111–113] as implemented in GAUSSIAN 03.[114,115] The molecular cavity was based on the united atom topological model applied on UAHF radii, optimized for the HF/6-31G(d) level.

Acknowledgements

The authors are grateful to the Fundo Europeu para o Desenvolvimento Regional, Fundação para a Ciência e Tecnologia (FCT), the POCI 2010 Programme, the Portuguese NMR Network (IST-UTL Center), PEst-OE/QUI/UI0100/2011, University of A Coruña and the Spanish-Portuguese Bilateral Programme (Acção Integrada E-56/05, Acción integrada HP2004-0074).

References

1 K. H. Thompson, J. H. McNeill and C. Orvig, *Chem. Rev.*, 1999, **99**, 2561–2571.
2 K. H. Thompson and C. Orvig, *J. Chem. Soc., Dalton. Trans.*, 2000, 2885–2892.
3 H. Sakurai, Y. Kojima, Y. Yoshikawa, K. Kawabe and H. Yasui, *Coord. Chem. Rev.*, 2002, **226**, 187–198.
4 H. Sakurai, *Chem. Rec.*, 2002, **2**, 237–248.
5 H. Sakurai, J. Fugono and H. Yasui, *Mini-Rev. Med. Chem.*, 2004, **4**, 41–48.
6 H. Sakurai, H. Yasui and Y. Adachi, *Expert Opin. Invest. Drugs*, 2003, **12**, 1189–1203.
7 A. Gorzsas, I. Andersson and L. Pettersson, *Eur. J. Inorg. Chem.*, 2006, 3559–3565.
8 K. H. Thompson and C. Orvig, *Dalton Trans.*, 2006, 761–764.
9 K. H. Thompson and C. Orvig, *J. Inorg. Biochem.*, 2006, **100**, 1925–1935.
10 H. Sakurai, A. Katoh and Y. Yoshikawa, *Bull. Chem. Soc. Jpn.*, 2006, **79**, 1645–1664.

11 D. Rehder, *Bioinorganic Vanadium Chemistry*, Wiley, Chichester, 2010.
12 M. Passadouro, A. M. Metelo, A. S. Melao, J. R. Pedro, H. Faneca, E. Carvalho and M. M. C. A. Castro, *J. Inorg. Biochem.*, 2010, **104**, 987–992.
13 A. M. Metelo, R. Perez-Carro, M. M. C. A. Castro and P. Lopez-Larrubia, *J. Inorg. Biochem.*, 2012, **115**, 44–49.
14 D. C. Crans, J. J. Smee, E. Gaidamauskas and L. Q. Yang, *Chem. Rev.*, 2004, **104**, 849–902.
15 P. Hulley and A. Davison, *J. Trace Elem. Exp. Med.*, 2003, **16**, 281–290.
16 M. Mahroof-Tahir, D. Brezina, N. Fatima, M. I. Choudhary and Atta-ur-Rahman, *J. Inorg. Biochem.*, 2005, **99**, 589–599.
17 H. S. Ou, L. M. Yan, D. Mustafi, M. W. Makinen and M. J. Brady, *J. Biol. Inorg. Chem.*, 2005, **10**, 874–886.
18 M. Li, W. J. Ding, B. Baruah, D. C. Crans and R. L. Wang, *J. Inorg. Biochem.*, 2008, **102**, 1846–1853.
19 K. G. Peters, M. G. Davis, B. W. Howard, M. Pokross, V. Rastogi, C. Diven, K. D. Greis, E. Eby-Wilkens, M. Maier, A. Evdokimov, S. Soper and F. Genbauffe, *J. Inorg. Biochem.*, 2003, **96**, 321–330.
20 D. Rehder, *Future Med. Chem.*, 2012, **4**, 1823–1837.
21 G. Heinemann, B. Fichtl, M. Mentler and W. Vogt, *J. Inorg. Biochem.*, 2002, **90**, 38–42.
22 B. D. Liboiron, K. H. Thompson, G. R. Hanson, E. Lam, N. Aebischer and C. Orvig, *J. Am. Chem. Soc.*, 2005, **127**, 5104–5115.
23 T. Jakusch, J. C. Pessoa and T. Kiss, *Coord. Chem. Rev.*, 2011, **255**, 2218–2226.
24 K. H. Thompson, B. D. Liboiron, Y. S. K. D. D. Bellman, I. A. Setyawati, B. O. Patrick, V. Karunaratne, G. Rawji, J. Wheeler, K. Sutton, S. Bhanot, C. Cassidy, J. H. McNeill, V. G. Yuen and C. Orvig, *J. Biol. Inorg. Chem.*, 2003, **8**, 66–74.
25 K. H. Thompson, J. Lichter, C. Lebel, M. C. Scaife, J. H. McNeill and C. Orvig, *J. Inorg. Biochem.*, 2009, **103**, 554–558.
26 P. W. Winter, A. Al-Qatati, A. L. Wolf-Ringwall, S. Schoeberl, P. B. Chatterjee, B. G. Barisas, D. A. Roess and D. C. Crans, *Dalton Trans.*, 2012, **41**, 6419–6430.
27 P. Caravan, L. Gelmini, N. Glover, F. G. Herring, H. L. Li, J. H. McNeill, S. J. Rettig, I. A. Setyawati, E. Shuter, Y. Sun, A. S. Tracey, V. G. Yuen and C. Orvig, *J. Am. Chem. Soc.*, 1995, **117**, 12759–12770.
28 M. Rangel, A. Leite, M. J. Amorim, E. Garribba, G. Micera and E. Lodyga-Chruscinska, *Inorg. Chem.*, 2006, **45**, 8086–8097.
29 H. Sakurai, A. Katoh, T. Kiss, T. Jakusch and M. Hattori, *Metallomics*, 2010, **2**, 670–682.
30 M. Rangel, M. J. Amorim, A. Nunes, A. Leite, E. Pereira, B. de Castro, C. Sousa, Y. Yoshikawa and H. Sakurai, *J. Inorg. Biochem.*, 2009, **103**, 496–502.
31 N. F. Olivieri, G. Koren, C. Hermann, Y. Bentur, D. Chung, J. Klein, P. Stlouis, M. H. Freedman, R. A. Mcclelland and D. M. Templeton, *Lancet*, 1990, **336**, 1275–1279.
32 Z. D. Liu and R. C. Hider, *Coord. Chem. Rev.*, 2002, **232**, 151–171.
33 L. E. Scott and C. Orvig, *Chem. Rev.*, 2009, **109**, 4885–4910.
34 M. Rangel, *Transition Met. Chem.*, 2001, **26**, 219–223.
35 P. Buglyo, T. Kiss, E. Kiss, D. Sanna, E. Garribba and G. Micera, *J. Chem. Soc., Dalton Trans.*, 2002, 2275–2282.
36 M. M. C. A. Castro, F. Avecilla, C. F. G. C. Geraldes, B. de Castro and M. Rangel, *Inorg. Chim. Acta*, 2003, **356**, 142–154.
37 M. M. C. A. Castro, C. F. G. C. Geraldes, P. Gameiro, E. Pereira, B. Castro and M. Rangel, *J. Inorg. Biochem.*, 2000, **80**, 177–179.
38 J. Burgess, B. DeCastro, C. Oliveira, M. Rangel and W. Schlindwein, *Polyhedron*, 1997, **16**, 789–794.
39 M. Rangel, A. Tamura, C. Fukushima and H. Sakurai, *J. Biol. Inorg. Chem.*, 2001, **6**, 128–132.
40 T. Jakusch, D. Hollender, E. A. Enyedy, C. S. Gonzalez, M. Montes-Bayon, A. Sanz-Medel, J. C. Pessoa, I. Tomaz and T. Kiss, *Dalton Trans.*, 2009, 2428–2437.
41 C. J. Sunderland, M. Botta, S. Aime and K. N. Raymond, *Inorg. Chem.*, 2001, **40**, 6746–6756.
42 H. Faneca, V. A. Figueiredo, I. Tomaz, G. Goncalves, F. Avecilla, M. C. P. de Lima, C. F. G. C. Geraldes, J. C. Pessoa and M. M. C. A. Castro, *J. Inorg. Biochem.*, 2009, **103**, 601–608.
43 T. Kiss, T. Jakusch, D. Hollender, A. Dornyei, E. A. Enyedy, J. C. Pessoa, H. Sakurai and A. Sanz-Medel, *Coord. Chem. Rev.*, 2008, **252**, 1153–1162.
44 A. K. Bordbar, A. L. Creagh, F. Mohammadi, C. A. Haynes and C. Orvig, *J. Inorg. Biochem.*, 2009, **103**, 643–647.
45 D. Sanna, E. Garribba and G. Micera, *J. Inorg. Biochem.*, 2009, **103**, 648–655.
46 D. Sanna, G. Micera and E. Garribba, *Inorg. Chem.*, 2010, **49**, 174–187.
47 T. Jakusch, A. Dean, T. Oncsik, A. C. Benyei, V. Di Marco and T. Kiss, *Dalton Trans.*, 2010, **39**, 212–220.
48 D. Sanna, L. Biro, P. Buglyo, G. Micera and E. Garribba, *Metallomics*, 2012, **4**, 33–36.
49 D. Sanna, P. Buglyo, A. I. Tomaz, J. C. Pessoa, S. Borovic, G. Micera and E. Garribba, *Dalton Trans.*, 2012, **41**, 12824–12838.
50 D. Sanna, L. Biro, P. Buglyo, G. Micera and E. Garribba, *J. Inorg. Biochem.*, 2012, **115**, 87–99.
51 H. Z. Sun, H. Y. Li and P. J. Sadler, *Chem. Rev.*, 1999, **99**, 2817–2842.
52 G. Colmenarejo, *Med. Res. Rev.*, 2003, **23**, 275–301.
53 M. H. Nagaoka, T. Yamazaki and T. Maitani, *Biochem. Biophys. Res. Commun.*, 2002, **296**, 1207–1214.
54 J. C. Pessoa and I. Tomaz, *Curr. Med. Chem.*, 2010, **17**, 3701–3738.
55 M. H. Nagaoka, H. Akiyama and T. Maitani, *Analyst*, 2004, **129**, 51–54.
56 K. De Cremer, M. Van Hulle, C. Chery, R. Cornelis, K. Strijckmans, R. Dams, N. Lameire and R. Vanholder, *J. Biol. Inorg. Chem.*, 2002, **7**, 884–890.

57 G. G. S. Mehtab, S. Roy, A. I. Tomaz, T. Santos-Silva, M. F. A. Santos, M. J. Romão, T. Jakusch, T. Kiss and J. C. Pessoa, *J. Inorg. Biochem.*, 2013, **121**, 187.
58 W. R. Carroll, P. Pellechia and K. D. Shimizu, *Org. Lett.*, 2008, **10**, 3547–3550.
59 L. N. Zekany and I. Nágypal, in *Computational Methods for the Determination of Stability Constants*, ed. D. Leggett, Plenum, New York, 1985, pp. 291–353.
60 R. G. Parr and W. Yang, *Density Functional Theory of Atoms and Molecules*, Oxford University Press, New York, 1989.
61 J. C. Pessoa and L. Vilas Boas, in *Comprehensive Coordination Chemistry*, ed. R. D. Gillard, J. A. McKleverty and M. G. Wilkinson, Pergamon, Oxford, 1987, vol. 3, pp. 453–583.
62 J. C. Pessoa, L. F. V. Boas, R. D. Gillard and R. J. Lancashire, *Polyhedron*, 1988, **7**, 1245–1262.
63 A. Rockenbauer and L. Korecz, *Appl. Magn. Reson.*, 1996, **10**, 29–43.
64 E. Garribba, G. Micera, E. Lodyga-Chruscinska and D. Sanna, *Eur. J. Inorg. Chem.*, 2006, 2690–2700.
65 K. Wuthrich, *Helv. Chim. Acta*, 1965, **48**, 1012–1017.
66 N. D. Chasteen, in *Biological Magnetic Resonance*, ed. J. Lawrence, L. J. Berlin and J. Reuben, Plenum, New York, 1981, pp. 53–119.
67 G. R. Hanson, Y. Sun and C. Orvig, *Inorg. Chem.*, 1996, **35**, 6507–6512.
68 T. Kiss, E. Kiss, G. Micera and D. Sanna, *Inorg. Chim. Acta*, 1998, **283**, 202–210.
69 J. C. Pessoa, L. F. V. Boas and R. D. Gillard, *Polyhedron*, 1989, **8**, 1173–1199.
70 J. C. Pessoa, R. L. Marques, L. F. V. Boas and R. D. Gillard, *Polyhedron*, 1990, **9**, 81–98.
71 J. C. Pessoa, S. M. Luz, R. Duarte, J. J. G. Moura and R. D. Gillard, *Polyhedron*, 1993, **12**, 2857–2867.
72 J. C. Pessoa, L. F. V. Boas and R. D. Gillard, *Polyhedron*, 1990, **9**, 2101–2125.
73 J. C. Pessoa, S. M. Luz, I. Cavaco and R. D. Gillard, *Polyhedron*, 1994, **13**, 3177–3198.
74 J. C. Pessoa, I. Tomaz, T. Kiss, E. Kiss and P. Buglyo, *J. Biol. Inorg. Chem.*, 2002, **7**, 225–240.
75 J. C. Pessoa, I. Tomaz, T. Kiss and P. Buglyo, *J. Inorg. Biochem.*, 2001, **84**, 259–270.
76 D. Sanna, P. Buglyo, G. Micera and E. Garribba, *J. Biol. Inorg. Chem.*, 2010, **15**, 825–839.
77 D. Mustafi, E. V. Galtseva, J. Krzystek, L. C. Brunel and M. W. Makinen, *J. Phys. Chem. A*, 1999, **103**, 11279–11286.
78 L. K. White and N. D. Chasteen, *J. Phys. Chem.*, 1979, **83**, 279–284.
79 D. C. S. Crans and J. J. Smee, in *Comprehensive Coordination Chemistry II*, ed. J. A. McCleverty and T. J. Meyer, Elsevier, Amsterdam, 2004, ch. 4, vol. 4 (ed. A. G. Wedd), pp. 176–279.
80 T. F. Toyoshima, M. Fujihara and S. Tamagaki, *J. Oleo Sci.*, 2002, **51**, 313–321.
81 G. Gran, *Acta Chem. Scand.*, 1950, 550–575.
82 P. Gans, A. Sabatini and A. Vacca, *Inorg. Chim. Acta*, 1983, **79**, 219–220.
83 L. Casella, M. Gullotti, A. Pintar, S. Colonna and A. Manfredi, *Inorg. Chim. Acta*, 1988, **144**, 89–97.
84 N. D. Chasteen, *Coord. Chem. Rev.*, 1977, **22**, 1–36.
85 N. D. Chasteen, J. K. Grady and C. E. Holloway, *Inorg. Chem.*, 1986, **25**, 2754–2760.
86 L. Vellenga, T. Wensing, H. J. A. Egberts, J. E. Vandijk, J. M. V. M. Mouwen and H. J. Breukink, *Vet. Res. Commun.*, 1989, **13**, 467–474.
87 B. Yuan, K. Murayama and H. Yan, *Appl. Spectrosc.*, 2007, **61**, 921–927.
88 *SHELXS-97, revision 5.1*, University of Gottingen, Gottingen, Germany, 1997.
89 G. M. Sheldrick, *SHELXL-97, revision 5.1*, University of Gottingen, Gottingen, Germany, 1997.
90 G. W. T. M. J. Frisch, H. B. Schlegel, G. E. Scuseria, M. A. Robb, J. R. Cheeseman, J. A. Montgomery Jr., T. Vreven, K. N. Kudin, J. C. Burant, J. M. Millam, S. S. Iyengar, J. Tomasi, V. Barone, B. Mennucci, M. Cossi, G. Scalmani, N. Rega, G. A. Petersson, H. Nakatsuji, M. Hada, M. Ehara, K. Toyota, R. Fukuda, J. Hasegawa, M. Ishida, T. Nakajima, Y. Honda, O. Kitao, H. Nakai, M. Klene, X. Li, J. E. Knox, H. P. Hratchian, J. B. Cross, C. Adamo, J. Jaramillo, R. Gomperts, R. E. Stratmann, O. Yazyev, A. J. Austin, R. Cammi, C. Pomelli, J. W. Ochterski, P. Y. Ayala, K. Morokuma, G. A. Voth, P. Salvador, J. J. Dannenberg, V. G. Zakrzewski, S. Dapprich, A. D. Daniels, M. C. Strain, O. Farkas, D. K. Malick, A. D. Rabuck, K. Raghavachari, J. B. Foresman, J. V. Ortiz, Q. Cui, A. G. Baboul, S. Clifford, J. Cioslowski, B. B. Stefanov, G. Liu, A. Liashenko, P. Piskorz, I. Komaromi, R. L. Martin, D. J. Fox, T. Keith, M. A. Al-Laham, C. Y. Peng, A. Nanayakkara, M. Challacombe, P. M. W. Gill, B. Johnson, W. Chen, M. W. Wong, C. Gonzalez and J. A. Pople, *GAUSSIAN 03 (Revision C.02)*, Gaussian Inc., Wallingford, CT, 2004.
91 L. R. W. J. Hehre, P. V. R. Schleyer and J. A. Pople, *Ab Initio Molecular Orbital Theory*, New York, 1986.
92 J. P. Perdew, *Phys. Rev. B: Condens. Matter*, 1986, **33**, 8822–8824.
93 J. P. Perdew, K. Burke and M. Ernzerhof, *Phys. Rev. Lett.*, 1997, **78**, 1396–1396.
94 R. Ditchfield, W. J. Hehre and J. A. Pople, *J. Chem. Phys.*, 1971, **54**, 724–728.
95 W. J. Hehre, R. Ditchfield and J. A. Pople, *J. Chem. Phys.*, 1972, **56**, 2257–2261.
96 P. C. Hariharan and J. A. Pople, *Mol. Phys.*, 1974, **27**, 209–214.
97 M. S. Gordon, *Chem. Phys. Lett.*, 1980, **76**, 163–168.
98 P. C. Hariharan and J. A. Pople, *Theor. Chim. Acta*, 1973, **28**, 213–222.
99 J. E. Carpenter and F. Weinhold, *J. Mol. Struct. (THEOCHEM)*, 1988, **46**, 41–62.

100 J. P. Foster and F. Weinhold, *J. Am. Chem. Soc.*, 1980, **102**, 7211–7218.
101 A. E. Reed and F. Weinhold, *J. Chem. Phys.*, 1983, **78**, 4066–4073.
102 A. E. Reed, R. B. Weinstock and F. Weinhold, *J. Chem. Phys.*, 1985, **83**, 735–746.
103 A. E. Reed and F. Weinhold, *J. Chem. Phys.*, 1985, **83**, 1736–1740.
104 A. E. Reed, L. A. Curtiss and F. Weinhold, *Chem. Rev.*, 1988, **88**, 899–926.
105 K. B. Wiberg, *Tetrahedron*, 1968, **24**, 1083–1096.
106 A. D. Mclean and G. S. Chandler, *J. Chem. Phys.*, 1980, **72**, 5639–5648.
107 R. Krishnan, J. S. Binkley, R. Seeger and J. A. Pople, *J. Chem. Phys.*, 1980, **72**, 650–654.
108 A. J. Wachters, *J. Chem. Phys.*, 1970, **52**, 1033–1036.
109 P. J. Hay, *J. Chem. Phys.*, 1977, **66**, 4377–4384.
110 K. Raghavachari and G. W. Trucks, *J. Chem. Phys.*, 1989, **91**, 1062–1065.
111 M. Cossi, V. Barone, B. Mennucci and J. Tomasi, *Chem. Phys. Lett.*, 1998, **286**, 253–260.
112 E. Cances, B. Mennucci and J. Tomasi, *J. Chem. Phys.*, 1997, **107**, 3032–3041.
113 B. Mennucci and J. Tomasi, *J. Chem. Phys.*, 1997, **106**, 5151–5158.
114 J. Tomasi, B. Mennucci and R. Cammi, *Chem. Rev.*, 2005, **105**, 2999–3093.
115 M. Cossi, G. Scalmani, N. Rega and V. Barone, *J. Chem. Phys.*, 2002, **117**, 43–54.